SPECIAL SECTION: ORIGINAL ARTICLE

Ocean Mixing Processes (OMIX): Impact on Biogeochemistry, Climate and Ecosystem

Elevated turbulent and double-diffusive nutrient flux in the Kuroshio over the Izu Ridge and in the Kuroshio Extension

Takeyoshi Nagai[1] · Gandy Maria Rosales Quintana[2] · Gloria Silvana Durán Gómez[1] · Fuminori Hashihama[1] · Kosei Komatsu[3]

Abstract

While the Kuroshio is known to be a nutrient stream, as these nutrients are in dark subsurface layers, they are not immediately available for photosynthesis unless they are supplied to the sunlit surface layers. Recent microstructure observations have revealed that strong diapycnal mixing caused by the Kuroshio flowing over topographic features and double diffusion in the subsurface layers of the Kuroshio. However, it is still unclear how much nutrient flux can be provided by these microscale mixing processes. In this study, using an autonomous microstructure float and nutrient samplings, nutrient flux caused by the Kuroshio over the Izu Ridge, and that caused by double diffusion in the Kuroshio Extension are quantified. The nitrate diffusive flux is estimated to be $> 1 \, \mathrm{mmol \, N \, m^{-2} day^{-1}}$ over a distance, 20–30 km near the Izu Ridge and $> 0.1 \, \mathrm{mmol \, N \, m^{-2} day^{-1}}$, which persists further downstream direction over 100 km along the Kuroshio, increasing the subsurface chlorophyll-a concentration in the region 200 km downstream. The double-diffusion-induced nitrate flux is estimated to be $1\text{-}10 \, \mathrm{mmol \, N \, m^{-2} day^{-1}}$ in the pycnostad $26\text{–}26.5 \, \mathrm{kg m^{-3}}$ of the Kuroshio Extension, suggesting that whether this double-diffusion-induced nutrient flux in the subsurface layers can ultimately contribute to surface primary production depends on additional eddy up- and northward fluxes.

Keywords The Kuroshio · Turbulence · Double-Diffusion · Izu-Ridge · The Kuroshio Extension

1 Introduction

The Kuroshio, a warm western boundary current in the North Pacific that flows along the south coast of Japan, is one of the strongest currents in the world ocean. It is a very distinctive current as it encounters many rough topographic features (Hasegawa *et al.* 2019). In the upstream regions, the Kuroshio hits Green Island and flows over the I-Lan Ridge east of Taiwan. After leaving Taiwan, it continues to flow northeastward on the continental slope of the Okinawa Trough. When the Kuroshio reaches the west of Kyushu, where the half-tube-like topography of the Okinawa Trough ends, it changes the flow direction from northeast to southeast. Then, the southeastward flowing Kuroshio, at the south of Kyushu, flows over many seamounts and sills in the Tokara Strait. After passing the Tokara Strait, the Kuroshio turns its direction again, from southeast to northeast, and reaches the regions south of Honshu. When the Kuroshio takes non-large meandering paths, the path modulations of the Kuroshio occur with timescales of weeks to months. These modulating paths frequently bring the strong current of the Kuroshio on the continental shelves and capes at different locations depending on its paths. Finally, the Kuroshio flows across the Izu Ridge before it flows away from the south of Japan to the Kuroshio Extension toward the east.

In these topographic features, several previous studies have reported that the Kuroshio induces strong turbulence and associated diapycnal mixing. Chang et al. (2016) observed large Kelvin–Helmholtz billows generated in the Kuroshio above the seamount near Green Island east of

✉ Takeyoshi Nagai
  takeyoshi@gmail.com

1 Department of Ocean Sciences, Tokyo University of Marine Science and Technology, Tokyo, Japan

2 Ocean and Earth Science, National Oceanography Centre Southampton, University of Southampton, Southampton, UK

3 Atmosphere and Ocean Research Institute, The University of Tokyo, Tokyo, Japan

Taiwan. Microstructure observations in the Tokara Strait, by Tsutsumi et al. (2017), found that the turbulent energy dissipation rates near the Kuroshio are larger on the downstream side of the strait compared to that in the upstream. Furthermore, Nagai et al. (2017) using a tow-yo microstructure profiler in the Tokara Strait found coherent banded layers of strong turbulence associated with the large amplitude high vertical wavenumber shear, caused by the near-inertial waves in the Kuroshio near seamounts. After passing over the rough topography in the upstream regions, the Kuroshio frequently approaches to the continental shelves south of Japan. In the Hyuganada Sea southeast of Kyushu, the tow-yo microstructure surveys by Nagai et al. (2019b) revealed that turbulent dissipation rates are elevated to $> \mathcal{O}(10^{-7} \, \mathrm{Wkg}^{-1})$ by trapped near-inertial internal waves over 20–30 km across the Kuroshio.

These elevated turbulence and vertical mixing induced by the Kuroshio flowing over topographic features not only dissipate the Kuroshio energy and modify the water masses, but also are mixing tracers including nutrients. Several previous studies have shown that the Kuroshio is a nutrient stream similar to the Gulf Stream (Pelegrí et al. 1996; Pelegrí and Csanady 1991), transporting a large amount of nutrients from tropical to the subpolar regions (Guo et al. 2012, 2013; Komatsu and Hiroe 2019; Nagai et al. 2019a). However, because these nutrient conduits lie in the dark subsurface layers, they are not immediately available for photosynthesis. The mixing processes over these topographic features along the Kuroshio are, therefore, important agents for supplying nutrients to the primary producers, which ultimately support higher tropic levels including large migratory fish species in the downstream Kuroshio Extension and subpolar regions (e.g., Durán Gómez et al. 2020).

To this end, Kaneko et al. (2012, 2013) conducted the microstructure observations with nutrient samplings in the Kuroshio Extension, and found that moderately enhanced turbulence in the Kuroshio thermocline induces a relatively large nitrate diffusive flux of $\mathcal{O}(0.1 \, \mathrm{mmol \, N \, m}^{-2} \mathrm{day}^{-1})$. On the other hand, above the rough topography in the upstream Kuroshio, Kobari et al. (2020) have shown that the strong turbulent mixing in the Tokara Strait induces a large amount of nitrate diffusive flux to the euphotic zone at a rate, $\mathcal{O}(1 \, \mathrm{mmol \, N \, m}^{-2} \mathrm{day}^{-1})$ on average. After flowing through the Tokara Strait, the Kuroshio frequently approaches to the continental shelf depending on the path. In the Hyuganada Sea, off southeast of Kyushu, Nagai et al. (2019a) showed that the Kuroshio flowing near the continental shelf elevates the turbulent diffusive nitrate flux as large as 1–10 mmol N m^{-2}day^{-1}. When the Kuroshio reaches the Izu Ridge, the flow encounters islands and sills within the ridge. Hasegawa et al. (2004) using a microstructure profiler, reported that very large turbulent energy dissipation rates of $\mathcal{O}(10^{-4} \, \mathrm{Wkg}^{-1})$ on the lee side of Aoga-shima Island, one of the islands in the Izu Ridge (Fig. 1a) associated with a sevenfold increase in nitrate concentration at 10 m depth compared to the region on the upstream side of the island. Tanaka et al. (2016) also reported a elevated nitrate diffusive flux in upper 300 m depth of $\mathcal{O}(1\text{-}10 \, \mathrm{mmol \, N \, m}^{-2} \mathrm{day}^{-1})$ near the sills in the Kuroshio over the Izu Ridge. However, because their observations are limited to the region very close proximity to the island or the sills in the Izu Ridge, how long the elevated turbulent intensity and the nutrient diffusive flux persist to the downstream direction is still unclear.

After the Kuroshio separates from the coast to the downstream Kuroshio Extension, because of the lack of shallow topographic features, strong turbulent mixing generated by the flow over a rough topography is absent. Although several studies have pointed out that the average turbulent energy dissipation rates are still moderately increased as large as $\sim 10^{-8} \, \mathrm{Wkg}^{-1}$ in the thermocline of the Kuroshio Extension (Nagai et al. 2012, 2015a; Kaneko et al. 2012), these values are 1–2 orders of magnitude less than that in the Kuroshio near the rough topography (Chang et al. 2016; Tsutsumi et al. 2017; Nagai et al. 2017). Thus, in the Kuroshio Extension, turbulent diapycnal mixing may not be as important as in the upstream region for mixing the water, away from the surface and bottom boundary layers. On the other hand, along the Kuroshio Extension, cold-fresh water can be frequently entrained into the jet caused by meso- and submesoscale stirring. Recent observations using an autonomous microstructure profiling float revealed that these lateral stirring processes with vertical shear generate vertical high wavenumber thermohaline interleaving structures in and below the thermocline of the Kuroshio Extension over 900 km (Nagai et al. 2015b). They also showed that intense microscale thermal variance dissipation occurred while turbulent kinetic energy (TKE) dissipation rates were relatively weak $< \mathcal{O}(10^{-8} \, \mathrm{Wkg}^{-1})$ in and below the Kuroshio Extension thermocline, suggesting that the double-diffusive convection is the dominant agent for the diapycnal mixing there. Although double-diffusive convection leads to the formation of new density layers like staircases, i.e., unmixing the density, it can exchange heat, salt and other tracers including nutrients vertically. Therefore, the enhanced double-diffusive convection observed in the Kuroshio Extension suggests that it can also induce large vertical nutrient fluxes. Oschlies et al. (2003) estimated salt-finger driven nutrient supply to the euphotic layer using a coarse resolution basin scale numerical model in the North Atlantic, and found that it can be as large as $\mathcal{O}(0.1 \, \mathrm{mol \, N \, m}^{-2} \mathrm{yr}^{-1})$ in the eastern North Atlantic, which is equivalent to $\mathcal{O}(0.1 \, \mathrm{mmol \, N \, m}^{-2} \mathrm{day}^{-1})$. However, because these estimates were derived from the rather coarse resolution model, the high vertical wavenumber thermohaline interleaving and associated large nutrient fluxes are most likely missing, underestimating the double-diffusive flux.

Fig. 1 Map of the surveys for (**a**) June 2017 cruise and (**b**) July 2013 cruise. In (**a**), color shading shows average satellite sea surface height during June 24–29, 2017. The white contour shows sea surface height at 0.5 m, and a white arrow represents the southernmost extent of the low sea surface height mentioned in the text. Black line indicates the ship track, blue and black triangles are the Navis-MR microstructure float and the Navis-BGC float profiling positions, respectively. Thin black contour shows topography of the Izu Ridge. White circles are the CTD-rosette sampling for nutrients. Mikura-jima and Aoga-shima are indicated as blue arrows and texts. In (**b**), color shading shows satellite sea surface temperature on 18 July 2013. Magenta and cyan curves are trajectories of the EM-APEX and Navis-MR float. Digits along the EM-APEX trajectory indicate days after the deployment. Black line represents across-front Underway-CTD transect shown in Fig. 10a
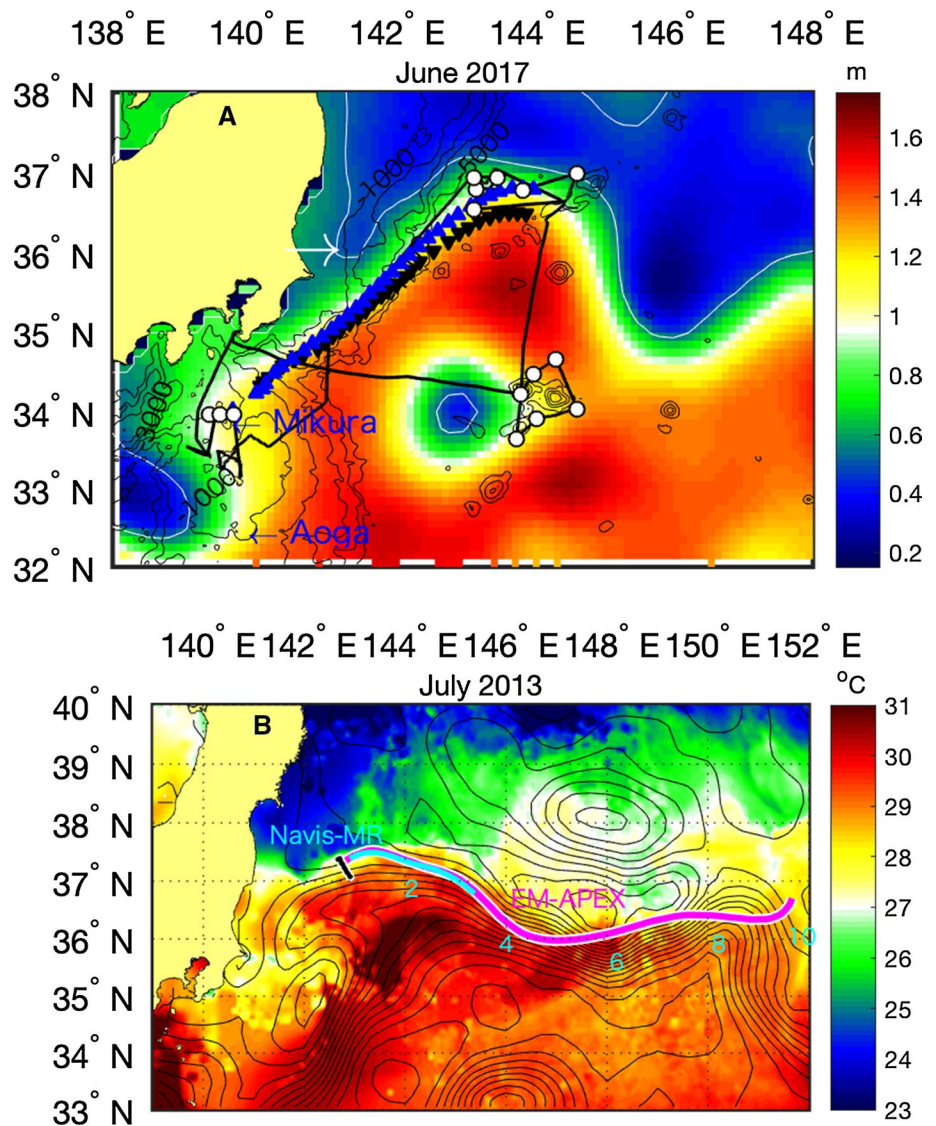
Dietze et al. (2004) estimated salt-finger-induced nitrate diffusive flux of 85 mmol N m^{-2}yr^{-1}, which is equivalent to the flux of $\mathcal{O}$(0.1 mmol N m^{-2}day^{-1}), using standard Conductivity Temperature Depth (hereinafter CTD) data in the eastern North Atlantic. However, because these estimates are obtained from the standard hydrographic data with a salt-finger parameterization, how well the parameterization reproduces the actual double-diffusive flux and whether double diffusion can actually occurs without being disrupted by the mechanical turbulence, are still unclear.

In this study, dataset from two research cruises in the Kuroshio and the Kuroshio Extension are analyzed. In both the surveys, an autonomous microstructure profiling float was deployed with other profiling floats equipped with the biogeochemical sensors and velocity measurable electromagnetic sensors, to measure continuously the microstructures and turbulence along the main stream of the Kuroshio

over the Izu Ridge and the Kuroshio Extension. The objectives of this study are to elucidate how much elevation of turbulent nutrient diffusive flux is induced by the Kuroshio flowing over the Izu Ridge, to understand how long this elevated nutrient flux near the Izu Ridge persists toward the downstream, and to quantify the double-diffusion-induced nutrient flux along the Kuroshio Extension using microstructure data. The paper is organized as follows. The Sect. 2 provides data and methods; the section 3 presents results from two different surveys. One is in the Kuroshio over the Izu Ridge, and the other is in the Kuroshio Extension. Discussion is given in the Sect. 4, which is followed by Summary and Conclusions in the Sect. 5.

2 Data and methods

In this study, the data from two observational campaigns are analyzed. One is conducted during July 2013 in the Kuroshio Extension using the R/V Kaiyo (JAMSTEC), and the other is in June 2017 in the Kuroshio near the Izu Ridge using the R/V Shinsei-maru (JAMSTEC). During these two cruises, several autonomous profiling floats including a microstructure float were deployed in the Kuroshio axis to make continuous measurements of turbulence and microstructure in the Kuroshio and the Kuroshio Extension.

2.1 Profiling float surveys in the Kuroshio over the Izu Ridge during June 2017

During the observations in June 2017, a cyclonic eddy generated from the Kuroshio Extension propagated westward direction, and interacted with the northward flowing Kuroshio, which was then bounced back to the middle of the Kuroshio recirculation gyre (Fig. 1). Two autonomous profiling floats were deployed at 34°N, 139.7°E in the Kuroshio flowing over the Izu Ridge in June 21 and recovered in June 27, 2017. One float is the autonomous microstructure float (hereinafter Navis-MR), which consists of a Navis Autonomous Profiling Float (Sea-Bird Scientific, Bellevue, WA USA) with a standard CTD (SBE41), the MicroRider and its battery pack (Rockland Scientific International Victoria, BC Canada). The MicroRider carries two shear probes and two high-resolution thermistors (FP07) to measure turbulent velocity shear and microscale temperature gradient, respectively. However, because the buoyancy pump of the Navis-MR was not operated properly, the mechanical noises generated by the buoyancy pump contaminated severely into shear probe data. Therefore, both turbulent kinetic energy dissipation rates and thermal variance dissipation rates were determined by fitting Kraichnan Spectra (Kraichnan 1968) with the temperature gradient spectra measured using FP07 thermistors. The other float is a Navis Autonomous Biogeochemical Float (hereinafter Navis-BGC, Sea-Bird Scientific, Bellevue, WA USA), which carries a CTD (SBE41), a fluorescence/backscattering/CDOM (ECO-MCOMS) sensor, and a dissolved oxygen (SBE63) sensor. The Navis-MR and the Navis-BGC obtained 34 and 30 vertical profiles over 520 km along the Kuroshio, respectively. Initially, the profiling depths for these floats were unexpectedly shallow as 200 m depth, due to the improper piston positions, which were modified to 450 m depth a few days after the deployments.

2.2 Profiling float surveys in the Kuroshio Extension during July 2013

Another observational campaign was conducted during July 2013 using autonomous profiling floats in the Kuroshio Extension Front. During this observation, the Kuroshio Extension flows along a relatively straight path. In this survey, the Navis-MR microstructure float and an ElectroMagnetic Autonomous Profiling Explorer (hereinafter EM-APEX) float were deployed at 37.3°N, 142.74°E in the first meander of the Kuroshio Extension front. After their deployments, they are rapidly advected by the Kuroshio Extension current toward the downstream regions. These two floats profiled over 4–500 m water columns every 2–3 hours along the Kuroshio Extension. The Navis-MR float obtained 14 microstructure profiles over 300 km along the Kuroshio Extension front before the recovery, 3 days after the deployment, and the EM-APEX float obtained 174 profiles of temperature, salinity and lateral flow over 900 km along the front in 10 days from its deployment (Fig. 1b). Before the float deployments, the Underway-CTD (Teledyne Oceanscience) was repeatedly deployed down to 500 m depth across the Kuroshio Extension front (Fig. 1b and 10a, c, e). The Underway-CTD probe carries a Sea-Bird CTD sensor to measure conductivity, temperature, and pressure, while it falls at a speed of 4 ms^{-1}.

During July 2013 observations, the microscale turbulent vertical shear data obtained by the Navis-MR were not contaminated by the buoyancy pump noise. Thus, the TKE dissipation rates are obtained using turbulent shear data acquired by two shear probes, and the microscale thermal variance dissipation rates are computed from microscale temperature gradient data measured by two FP07 thermistors.

2.3 Turbulent kinetic energy dissipation rate and eddy diffusivity

Assuming the isotropic turbulence, the TKE dissipation rates ϵ can be determined by turbulent shear variance $\overline{(d\mathbf{u}/dz)^2}$, which can be obtained by integrating the measured turbulent shear spectra, i.e.,

$$\epsilon = \frac{15}{4}\nu\left[\overline{\left(\frac{du}{dz}\right)^2} + \overline{\left(\frac{dv}{dz}\right)^2}\right],$$

$$\overline{\left(\frac{d\mathbf{u}}{dz}\right)^2} = \int_{k_o}^{k_c} \phi_{d\mathbf{u}/dz}dk,$$

(1)

where **u** is horizontal turbulent velocity vector, which consists of two horizontal velocity components u and v, normal to each other, z the vertical coordinate, ν the kinematic viscosity of seawater (m^{2}s^{-1}), $\phi_{d\mathbf{u}/dz}$ the wavenumber spectrum

of shear, k the vertical wavenumber, and k_o and k_c determine the wavenumber range of the integration with the lowest $k_o = 1$ cpm and the highest k_c wavenumber. The turbulent vertical shear du/dz and dv/dz are measured by two shear probes oriented normal to each other. The cutoff highest wavenumber k_c is ideally the Kolmogorov wavenumber, $(\epsilon/\nu^3)^{1/4}/2\pi$. However, since electronic noises often contaminate the shear data at the high wavenumber range and low frequency motion of the instrument by flow induces noises at low wavenumbers, these cutoff wavenumbers are set to avoid integrating these noises. The Nasmyth spectra (Nasmyth 1970) are integrated instead of the measured shear spectra for the outside the wavenumber range for the integration ($k < k_o$ and $k_c < k$). The data segment for 16 seconds, which corresponds to 8192 data points, is used to compute a shear spectrum. The free rising speed of the float ranges 0.11–0.26 ms^{-1}, which yields the vertical bin size for each dissipation rate measurement to be 1.76–4.16 m.

Using the measured TKE dissipation rates ϵ, the eddy diffusivity K_ρ for density can be computed following Osborn (1980) by

$$K_\rho = \gamma \frac{\epsilon}{N^2}, \tag{2}$$

where the mixing efficiency factor γ is assumed to be a constant value 0.2, and $N^2 = -g/\rho_o (d\rho/dz)$ is the buoyancy frequency square with g the gravitational acceleration, ρ and ρ_o are the density of seawater and its reference value, respectively.

2.4 Thermal variance dissipation rate and effective thermal diffusivity

The Navis-MR carries two FP07 thermistors to measure microscale temperature gradient. The microscale thermal variance dissipation rate χ is determined by the variance of the microscale temperature gradient, which can be obtained by integrating temperature gradient spectra,

$$\chi = 6k_T \overline{\left(\frac{dT}{dz}\right)^2},$$
$$\overline{\left(\frac{dT}{dz}\right)^2} = \int_{k_o}^{k_c} \phi_{dT/dz} dk, \tag{3}$$

where k_T is the molecular diffusivity for heat (m^{2}s^{-1}), dT/dz the microscale temperature vertical gradient, and $\phi_{dT/dz}$ the wavenumber spectrum of the temperature vertical gradient. Similar to the integration of the shear spectra, the integration range ($k_o < k < k_c$) is modified when the noises contaminate into the signals. Once χ is determined, the Kraichnan spectrum (Kraichnan 1968) is fitted to the computed spectra by the maximum likelihood method (Ruddick et al. 2000)

for various dissipation rates ϵ. For the data obtained during June 2017 observations, this spectral fitting method is used also for obtaining the TKE dissipation rates ϵ instead of the shear spectral method (1), since the turbulent shear data were contaminated by noises from the buoyancy pump of the Navis-MR float.

Based on the microscale thermal variance equation, using measured χ, the effective thermal diffusivity can be obtained simply by,

$$K_\theta = \frac{\chi}{2(\Theta_z)^2}, \tag{4}$$

where Θ_z is the mean background temperature vertical gradient (Osborn and Cox 1972).

2.5 Estimation of nutrient flux

The autonomous profiling floats deployed in this study do not carry nutrient sensors. Therefore, the nutrient samples obtained by the CTD-rosette water sampler were used to establish the relationship between water density and concentrations of nitrate and phosphate. These water samples were obtained at 15 stations near the Kuroshio, the Kuroshio Extension, and at the edge of the cyclonic eddy during June 2017 cruise (Fig. 1a). The samples taken at relatively deep layers (> 100 m depth) are analyzed using an AutoAnalyzer (QuAAtro 2-HR, BLTech), and those taken at shallower depth (< 100 m depth) are analyzed using a highly sensitive method for the determination of nanomolar nutrients in seawater (Hashihama et al. 2009; Hashihama 2013). These measured nutrient concentrations show increasing trends with denser water both for nitrate and phosphate (Fig. 2). The data are bin-averaged as a function of water density, and this relationship is used to interpolate and estimate the nitrate and phosphate concentrations at measured seawater density values by the autonomous floats. The 95% confidence intervals for the mean become narrower for the less dense water samples, suggesting that the accuracy of the estimated nutrient concentrations is better for less dense water near the Kuroshio and the Kuroshio Extension. Although the nutrient samples were collected in three different regions, the Izu Ridge, the Kuroshio Extension, and the edge of the cold core eddy, they show very similar relation with the density. This is probably because the former two regions are very close to the Kuroshio axis, and the cold core eddy was pinched off from the Kuroshio Extension. The same method was also tested using the data taken in the periodic nutrient observations conducted across the Kuroshio Extension by Japan Meteorological Agency, showing the same orders of magnitude in the nitrate diffusive flux.

Fig. 2 Nitrate and phosphate concentrations as a function of σ_θ measured during the cruise June 2017. Black lines are the bin-average nitrate (**a**) and phosphate (**b**) that are used to estimate nutrient concentrations from density measured by the autonomous float. The individual nutrient samples are shown for (green circle) those taken in the Izu Ridge, (magenta square) at the edge of the cold core eddy, and (blue triangles) in the Kuroshio Extension
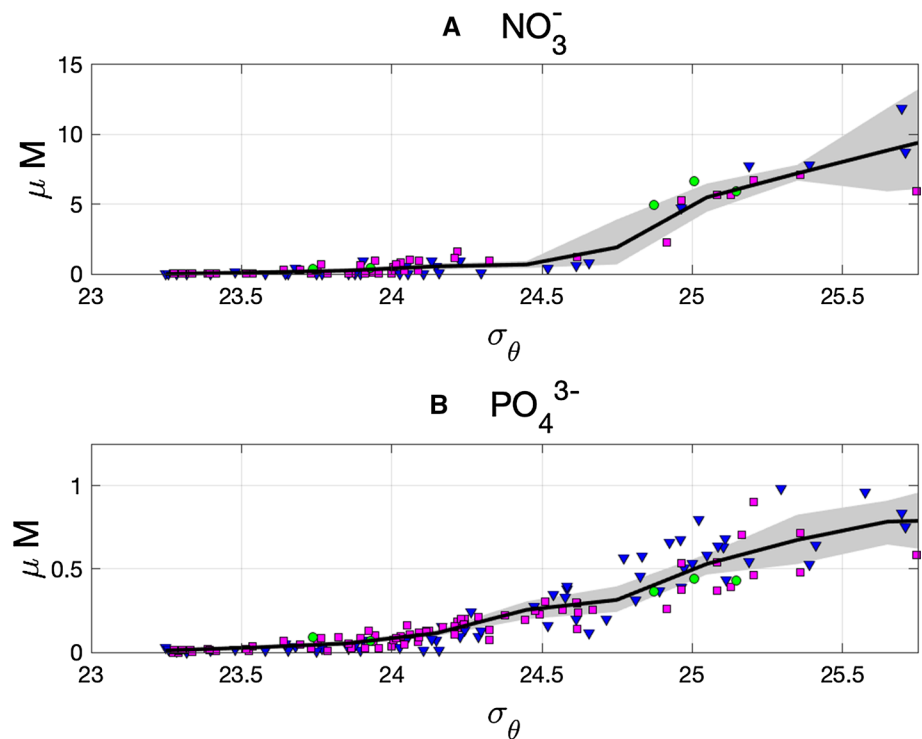
The vertical diffusive flux of nitrate and phosphate are then computed with two diffusivities as,

$$
\begin{aligned}
F_\rho^{NO_3^-} &= - K_\rho \frac{\partial NO_3^-}{\partial z}, \\
F_\theta^{NO_3^-} &= - K_\theta \frac{\partial NO_3^-}{\partial z}, \\
F_\rho^{PO_4^{3-}} &= - K_\rho \frac{\partial PO_4^{3-}}{\partial z}, \\
F_\theta^{PO_4^{3-}} &= - K_\theta \frac{\partial PO_4^{3-}}{\partial z},
\end{aligned}
\tag{5}
$$

where $\partial NO_3^- / \partial z$ and $\partial PO_4^{3-} / \partial z$ are vertical gradients of nitrate and phosphate.

2.6 Parameterizations of the double-diffusion-induced thermal diffusivity

In this study, the effects of the double-diffusive convection on the nutrient supply are considered in addition to that caused by turbulent mixing. The double-diffusion favorable thermal and saline conditions can be detected by density ratio, R_ρ,

$$
R_\rho = \frac{\alpha \Theta_z}{\beta S_z},
\tag{6}
$$

where α and β are heat and salt expansion coefficients, respectively, and S_z the mean salinity vertical gradient. When

the R_ρ close to 1, the conditions are favorable for salt-finger and diffusive convection.

However, in some occasions, interpreting R_ρ encounters some difficulties, as it has the singularity when salinity becomes homogeneous, which can be avoided using Turner angle Tu (Ruddick 1983; Radko 2013),

$$
Tu = \arctan \left(\frac{\alpha \delta \Theta + \beta \delta S}{\alpha \delta \Theta - \beta \delta S} \right),
\tag{7}
$$

where arctan is the arctangent, and $\delta \Theta$ and δS are the temperature and the salinity changes with depth, respectively. When $45° < Tu < 90°$, thermal and saline distributions are favorable for occurrence of the salt-finger, while when $-90° < Tu < -45°$, they are diffusive convection favorable conditions. The Turner angle Tu is computed for the data obtained by the autonomous profiling floats and the Underway-CTD.

Previous studies attempted to model the double-diffusion-induced diffusivity. These parameterizations use the density ratio R_ρ. In this study, to estimate the double-diffusion-induced thermal diffusivity and compare that with the observed ones using microstructure profiler data, two parameterizations developed by Radko and Smith (2012) and Fedorov (1988) are employed for salt-finger and diffusive convection case, respectively.

Radko and Smith (2012) modeled the salt-finger-induced thermal diffusivity as,

$$F_s = \frac{a_s}{\sqrt{R_\rho - 1}} + b_s$$

$$\Gamma = a_g \exp(-b_g R_\rho) + c_g \tag{8}$$

$$K_\theta^{Radko} = F_s k_T \Gamma,$$

where $a_s = 135.7$, $b_s = -62.75$, $a_g = 2.709$, $b_g = 2.513$, $c_g = 0.5128$ are all constants and $R_\rho > 1$ for salt-finger.

On the other hand, Fedorov (1988) developed the model for thermal diffusivity caused by diffusive convection as,

$$K_\theta^{Fedo} = 0.909\nu \exp\left(4.6 \exp\left[-0.54\left(\frac{1}{R_\rho} - 1\right)\right]\right), \tag{9}$$

where $0 < R_\rho < 1$ for diffusive convection.

Even with the vertical layering of temperature and salinity favorable for the occurrence of the double-diffusive convection, strong turbulent mixing can disrupt the double diffusion. To evaluate the importance of turbulence, non-dimensional numbers such as Richardson number, Ri and buoyancy Reynolds number, Re_b are computed using the data obtained by the autonomous profiling float, the Underway-CTD, and the shipboard ADCP. The Richardson number Ri is computed by

$$Ri = \frac{N^2}{U_z^2 + V_z^2}, \tag{10}$$

where U_z and V_z are the vertical shear of the zonal and meridional flows, respectively, measured by the EM-APEX float and the shipboard ADCP. When $Ri < 0.25$, the flow is known to be unstable for Kelvin–Helmholtz instability, leading to the microscale turbulence.

Depending on the strength of the turbulence and the stratification, the turbulent overturning eddies can be unable to induce vertical buoyancy flux. In such cases, double-diffusive convection can still be effective to induce vertical fluxes of heat and salt. To measure the ability of the turbulent overturns to induce buoyancy flux, and to disrupt the double diffusion, the buoyancy Reynolds number is computed as

$$Re_b = \frac{\epsilon}{\nu N^2}. \tag{11}$$

When $Re_b < 200$, the turbulence becomes no longer isotropic, and when $Re_b < 20$ the turbulent eddies no longer support buoyancy vertical flux (Yamazaki 1990).

3 Results

3.1 Thermohaline structures in the Kuroshio near the Izu Ridge

After the deployment, the Navis-MR and Navis-BGC were advected rapidly by the Kuroshio Current along nearly the same trajectory until they reached the region near 35°N, 141°E (Fig. 1). After they passed this point, trajectories of two floats started to diverge, and the Navis-MR profiled slightly colder side of the Kuroshio; whereas, the Navis-BGC profiled warmer side of the front. The distance between these two floats increased as large as 34.8 km at the last profiles in the crest of the first meander of the Kuroshio Extension.

Vertical sections of temperature and salinity measured along these trajectories of the floats show similar thermal and saline distributions northeast of the Izu Ridge (Fig. 3a-b). Both temperature sections show isothermal convex upward structures around 35.5°N. Because temperature dominantly determines density over salinity in this region, isopycnal shows also convex upward structures. At the same location, the salinity shows relatively lower values (34.5 PSU) than that of ambient waters (34.8 PSU) along the same isostad, $\sigma_\theta = 23.5$–25 (Fig. 3c–d). This low salinity filament like structures spread across the density layers around 25–150 m depth and 35.4–36°N, suggesting the lateral stirring caused by ambient subinertial flows, similar to the previous study (Nagai et al. 2015b). The low salinity interleaving layers are more frequently found in the section obtained by the Navis-MR float, which went on the slightly colder side of the front (e.g., 34–35°N and 36–36.75°N Fig. 3d). The position of the clearest low salinity interleaving at 35.5°N coincides with the region where the southernmost edge of the relatively low sea surface height reaches and encounters the northeastward flowing Kuroshio (see the white arrow and the contour in Fig. 1a). This is probably caused by the first branch of the cold-fresh coastal Oyashio, suggesting that the salinity interleaving structures are created by lateral stirring and entrainment of cold-fresh water from north into the Kuroshio mainstream.

3.2 Biogeochemical tracers in the Kuroshio near the Izu Ridge

The biogeochemical sensors equipped on the Navis-BGC float allowed us to measure also chlorophyll-a concentration, volume backscattering function and dissolved oxygen along the Kuroshio axis. The chlorophyll-a concentration shows high values ($> 1 \mu gL^{-1}$) at the same location where the low salinity interleaving is found with the convex upward isopycnal structures at 35.5°N (Fig. 4a). Similarly, the volume
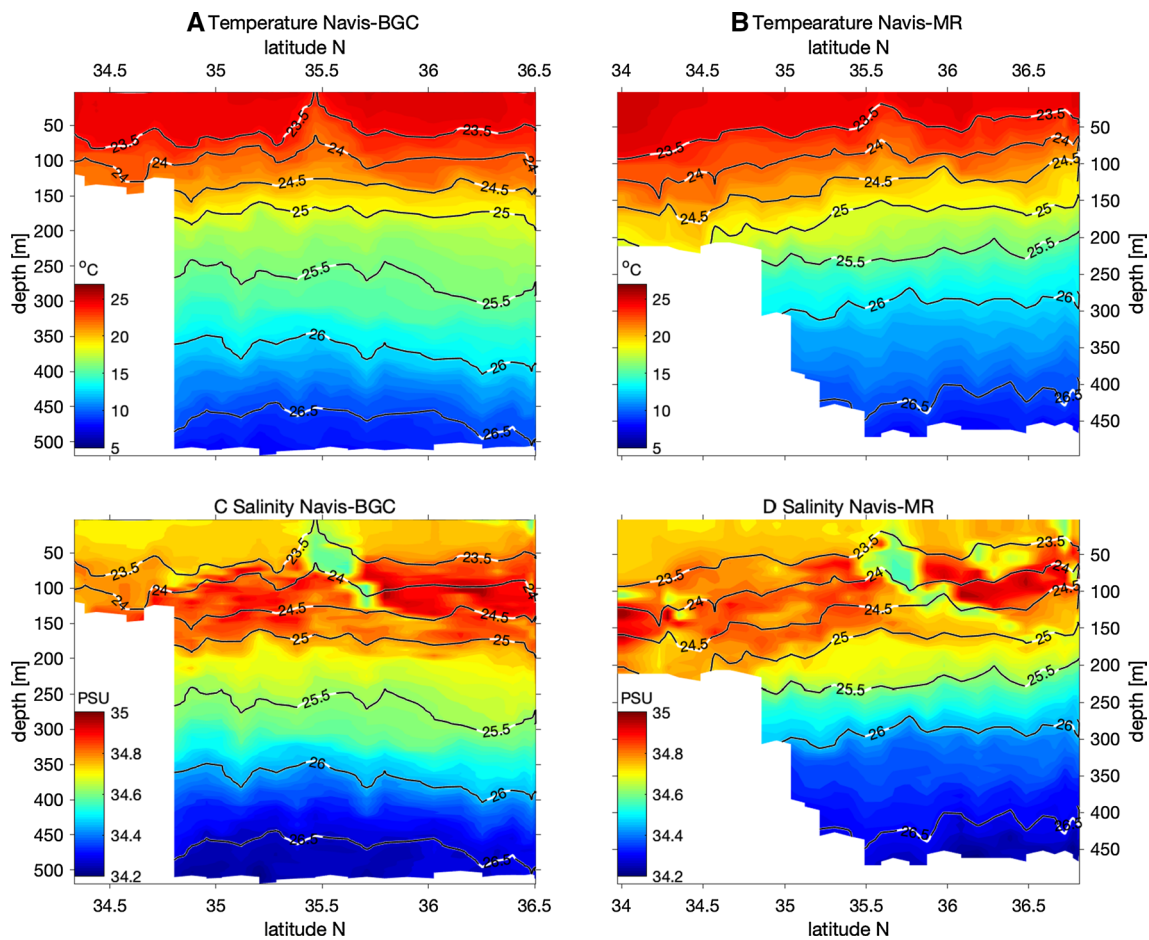
Fig. 3 Vertical sections of (**a–b**) temperature and (**c–d**) salinity measured using (**a** and **c**) the Navis-BGC and (**b** and **d**) the Navis-MR float. Black contours are isopycnals

backscattering function shows relatively higher values in the regions of high chlorophyll-a concentration (Fig. 4b). Besides these peaks in the chlorophyll-a concentration and the volume backscattering function at 35.5°N, they show relatively higher values in the region north of 35.4°N than that of southern region (Fig. 4a-b), suggesting that the amount of particulate organic matter including phytoplankton is relatively higher in the downstream region, north of 35.4°N. On the other hand, the dissolved oxygen concentration shows higher values near the surface without any clear influence from the higher amount of phytoplankton deduced from the chlorophyll-a concentration data (Fig. 4c). The higher chlorophyll-a concentration, which coincides with the low salinity water interleaving, may imply that the Oyashio influenced cold-fresh water brought the water of higher chlorophyll-a concentrations. However, the higher chlorophyll-a concentrations tend to appear along isopycnal (Fig. 4a), whereas the low salinity signature penetrates across the density layers (Fig. 3c–d). The temperature–salinity diagram with chlorophyll-a concentration with color shows clearly

that the higher chlorophyll-a concentration aligns isopycnals of $\sigma_\theta = 23.25$–24.25 without clear dependence on the salinity (Fig. 5a). The correlation coefficient between salinity and chlorophyll-a concentration, which exceeds 0.1 μgL^{-1} is low, −0.3. These results imply that the higher chlorophyll-a concentration is maintained also by other mechanisms in addition to the lateral advection of cold-fresh chlorophyll-rich waters.

3.3 Turbulence and microstructures in the Kuroshio near the Izu Ridge

TKE dissipation rates, ϵ and microscale thermal variance dissipation rates χ measured by the Navis-MR show elevated values in the region close to the Izu Ridge over the distance of 50–100 km (Fig. 6). The TKE dissipation rates ϵ in the south-westernmost region (34-34.75°N) show values above $\mathcal{O}(10^{-7}\ \mathrm{Wkg}^{-1})$ frequently and exceed $\mathcal{O}(10^{-6}\ \mathrm{Wkg}^{-1})$ at some locations near the surface (Fig. 6c). Average TKE dissipation rates from 40 to 200 m depth show that the depth
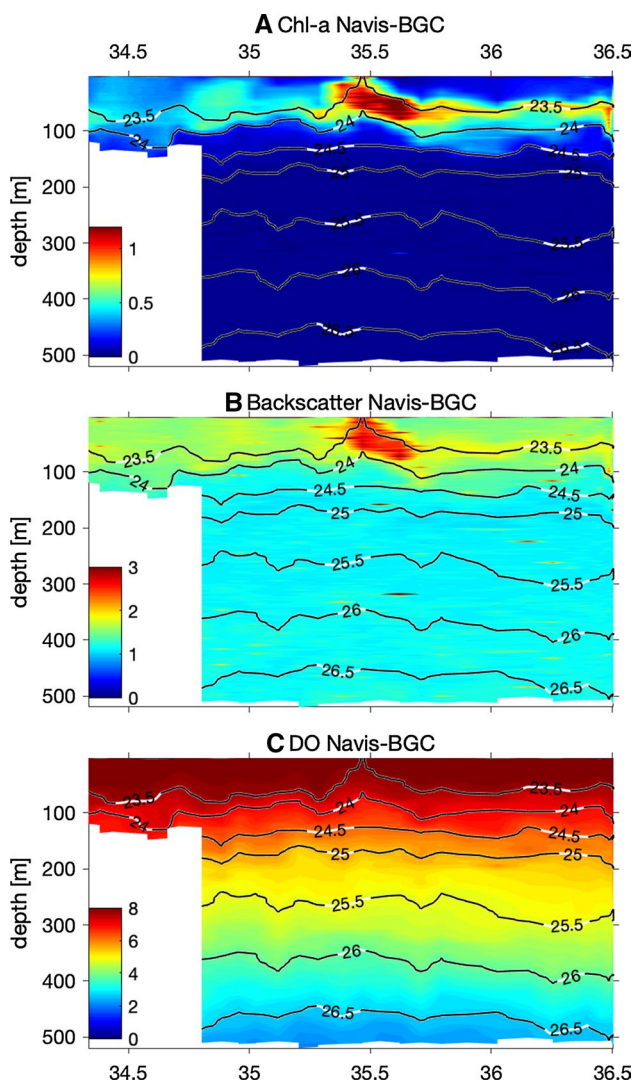
Fig. 4 Vertical sections of (**a**) chlorophyll-a [μgL^{-1}], (**b**) volume backscattering function [m^{-1}sr^{-1}], and (**c**) dissolved oxygen [mgL^{-1}] measured using the Navis-BGC float. Black contours are isopycnals

average dissipation rates are larger than $\mathcal{O}(10^{-6}\,\mathrm{Wkg}^{-1})$ in the region 34-34.4°N (Fig. 6a). These dissipation rates near the Izu Ridge and continental shelf off Boso Peninsula over a distance of $\sim 100\,\mathrm{km}$ are much larger than that in the downstream region by 2–3 orders of magnitude. Similarly, microscale thermal variance dissipation rates χ show very large values of $\mathcal{O}(10^{-6}\,°\mathrm{C}^2\mathrm{s}^{-1})$ in the same region where the large TKE dissipation rates are found in the south-western-most part (Fig. 6d). Average thermal variance dissipation rates from 40 to 200 m depth within 100 km from the south-westernmost part are 1–2 orders of magnitude greater than that in the downstream regions (Fig. 6b).

Assuming a constant mixing efficiency coefficient, $\gamma = 0.2$, and the steady state TKE balance among its

production, buoyancy destruction and dissipation terms, the eddy diffusivity K_ρ can be computed using (2) with the measured TKE dissipation rates and the background buoyancy frequency. The computed eddy diffusivity K_ρ shows larger values of $> \mathcal{O}(10^{-4}\,\mathrm{m}^2\mathrm{s}^{-1})$ within 100 km from the south-westernmost part of the transect (Fig. 7c), where the TKE dissipation rates ϵ are also large (Fig. 6c). Using the microscale thermal variance dissipation rates, the effective thermal diffusivity K_θ can also be obtained by (4). The computed thermal diffusivity shows a similar pattern having lager values closer to the Izu Ridge and the continental shelf off Boso Peninsula (Fig. 7d). Average eddy diffusivity K_ρ and effective thermal diffusivity K_θ from 40 to 200 m depth also show similar patterns of increasing trend toward the south-westernmost region close to the Izu Ridge (Fig. 7a–b). It should be noted, however, that the effective thermal diffusivity tends to show larger values than the eddy diffusivity in the regions 34–34.4°N and 35.6°N by several factors.

3.4 Diffusive nitrate flux near the Izu Ridge

The autonomous observations show that large TKE dissipation rates and diffusivities are found in the Kuroshio near the Izu Ridge and along the continental shelf of the Boso Peninsula. These microscale mixing processes can induce diapycnal flux of nutrients, supplying them from the subsurface nutrient stream toward the sunlit surface layers. Because the Navis-BGC float does not carry a nitrate sensor, nutrient concentrations are estimated from the relations between density and nutrients based on the water samplings (Figs. 2 and 8a). The derived diffusive vertical fluxes of nitrate using the eddy diffusivity $F_\rho^{NO_3^-}$ and the effective thermal diffusivity $F_\theta^{NO_3^-}$ show similar magnitudes and spatial patterns (Figure 8B and C). The large diffusive nitrate flux of $> \mathcal{O}(1\,\mathrm{mmol\,N\,m}^{-2}\mathrm{day}^{-1})$ is found in the south-westernmost part of the transect close to the Izu Ridge, which gradually decreases toward downstream, but accompanied by thin layers of relatively large nitrate flux $\sim \mathcal{O}(1\,\mathrm{mmol\,N\,m}^{-2}\mathrm{day}^{-1})$ persisting below 100 m depth (Fig. 8b and c). Average diffusive fluxes of nitrate and phosphate in 50–125 m depth as a function of latitude demonstrate clearly the elevated fluxes near the Izu Ridge (Fig. 9). The diffusive nutrient fluxes $F_\rho^{NO_3^-}$ and $F_\theta^{NO_3^-}$ show similar magnitudes and spatial distributions. However, the diffusive fluxes of both nitrate and phosphate with K_θ, ($F_\theta^{NO_3^-}$ and $F_\theta^{PO_4^{3-}}$) show 1–2 orders of magnitude larger values than that with K_ρ ($F_\rho^{NO_3^-}$ and $F_\rho^{PO_4^{3-}}$) at 35.6°N. This location coincides with the low salinity water interleaving structure (Fig. 3c–d).
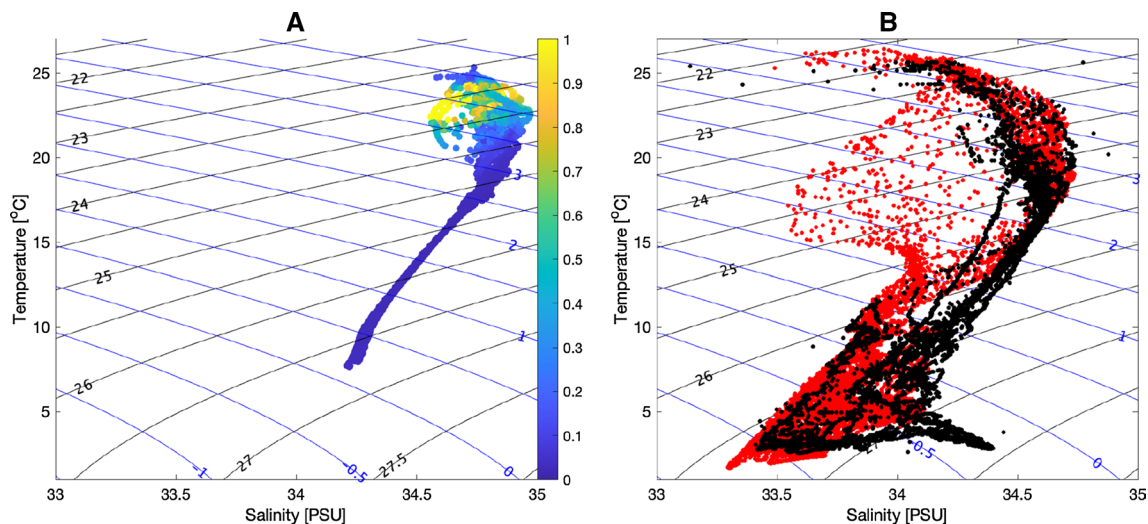
Fig. 5 Temperature–Salinity diagram for (**a**) June 2017 and (**b**) July 2013 cruises. Red and black points indicate data obtained by the EM-APEX float and the Underway-CTD, respectively in (**b**). The color shading in (**a**) indicates chlorophyll-a concentration [μgL^{-1}]. Black and blue contours are for isopycnals and isolines of the spiciness (Flament 2002), respectively

3.5 Observations in the Kuroshio Extension

After the Kuroshio flows over the Izu Ridge, the current is separated from the coast of Japan, changing its direction eastward to become the Kuroshio Extension. As it flows eastward, the bottom depth increases and the current no longer encounters the topographic obstacles. Therefore, chance of very strong turbulent energy dissipation occurrence $\epsilon \sim \mathcal{O}(10^{-7}\,\mathrm{Wkg}^{-1})$ in the subsurface layers becomes much less than that in the upstream regions where the Kuroshio can interfere directory with the topography, although moderate elevation of the TKE dissipation rates have been reported by a number of studies in the Kuroshio thermocline (Nagai et al. 2009; Kaneko et al. 2012; Nagai et al. 2012, 2015a). The autonomous float observations during July 2013 cruise (Nagai et al. 2015b) show characteristic thermohaline interleaving structures in and below the thermocline along the Kuroshio Extension over 900 km (Fig. 10c–f). Nagai et al. (2015b) showed that these interleaving layers are generated by lateral stirring and vertical shearing of cold-fresh Oyashio influenced water on the north and warm-salty Kuroshio water on the south side of the Kuroshio Extension (Fig. 3b). This thermohaline interleaving creates vertical inversions of temperature and salinity in the subsurface layer with the 100 m vertical wavelength, which are accompanied with the double-diffusive favorable Tuner angles Tu in the subsurface layer over 900 km (Fig. 11a–b).

The computed eddy diffusivity K_ρ and the effective thermal diffusivity K_θ using the Navis-MR microstructure float data obtained during July 2013 cruise (Fig. 1b), show much larger K_θ than K_ρ below 150 m depth (Fig. 12a–b). The much larger K_θ than K_ρ with double-diffusion favorable Tu suggests

that double-diffusive convection is the dominant agent for diapycnal mixing in these interleaving layers. This is also the case for the diapycnal mixing of the subsurface nutrients carried by the Kuroshio nutrient stream. Using these diffusivities and the model nitrate as a function of σ_θ (Fig. 2a), the nitrate diffusive vertical flux is also estimated for the Navis-MR data during July 2013 cruise. The estimated diffusive nitrate flux shows peaks between 200–300 m depth for both the estimations with the eddy diffusivity K_ρ and the effective thermal diffusivity K_θ (Fig. 12d–f). The magnitude of the diffusive flux is, however, 1–2 orders of magnitude larger with K_θ, 1-10 mmol N m^{-2}day^{-1} than that with K_ρ, 0.1-1 mmol N m^{-2}day^{-1}, reflecting the 1–2 orders of magnitude larger K_θ than K_ρ. These results suggest that double-diffusive convection plays a dominant role in diapycnal mixing of nutrients in the subsurface layers of the Kuroshio Extension.

4 Discussion

The results from the June 2017 cruise show elevated turbulent diffusive nutrient flux near the Izu Ridge in the Kuroshio. The diffusive nitrate flux is estimated to be $> \mathcal{O}(1\,\mathrm{mmol\,N\,m^{-2}day^{-1}})$ within 20–30 km from the southwesternmost profile of the Navis-MR, and reduced to $\mathcal{O}(10^{-2}\,\mathrm{mmol\,N\,m^{-2}day^{-1}})$ at 100 km away. Hasegawa et al. (2004) showed very strong turbulent energy dissipation rate $\mathcal{O}(10^{-4}\,\mathrm{Wkg}^{-1})$ in the vicinity of one of the islands in the Izu-Ogasawara Ridge, Aoga-shima Island (Fig. 1a). They also found that the sevenfold increase of nitrate concentration at 10 m depth in the lee side compared with that in the upstream side of the island. The distance between these
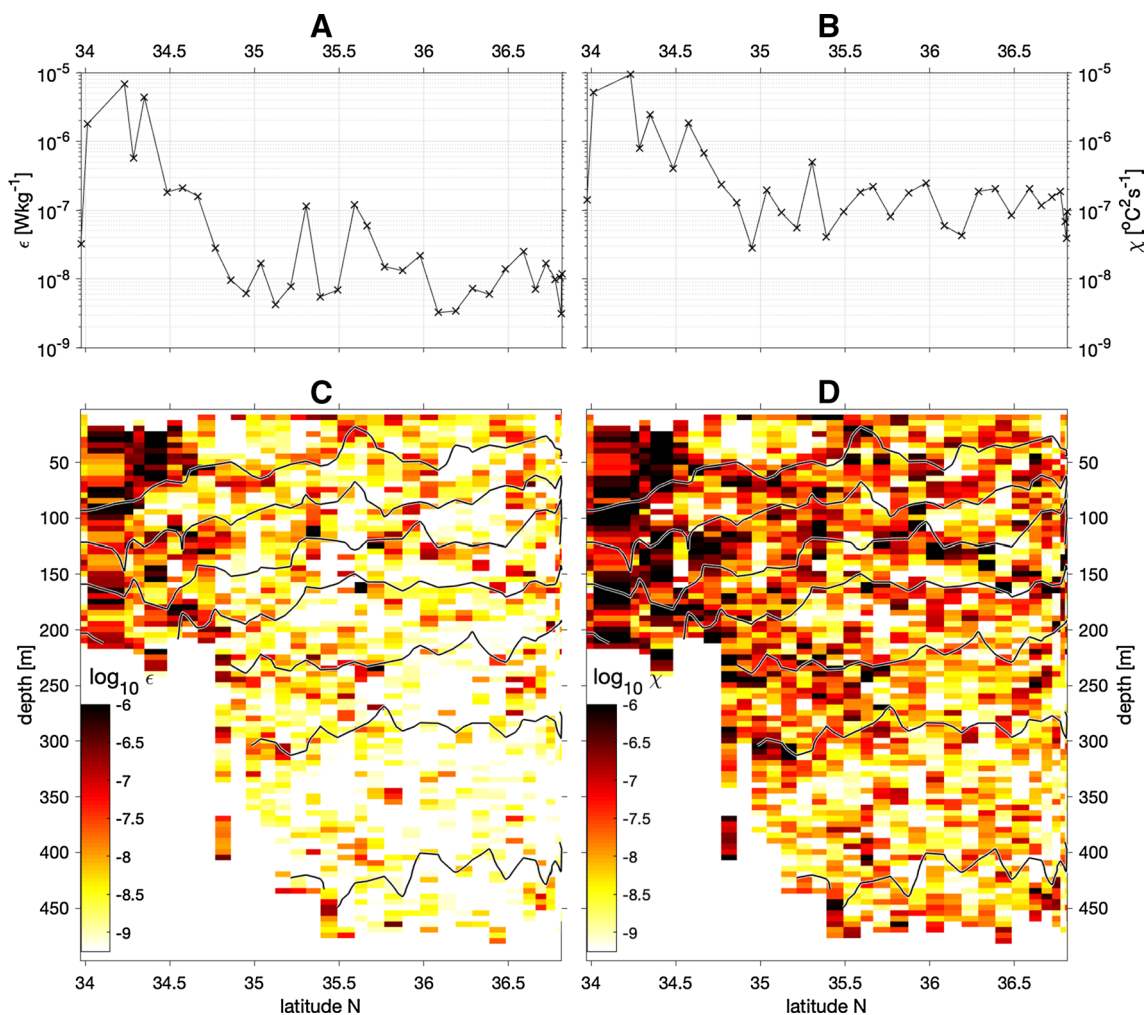
Fig. 6 Turbulent kinetic energy dissipation rate, ϵ [Wkg^{-1}] and microscale thermal variance dissipation rate, χ [^{o}C^{2}s^{-1}]. Mean (**a**) ϵ and (**b**) χ averaged between 40 and 200 m depth as a function of latitude. Vertical sections for (**c**) ϵ and (**d**) χ. The values are shown in log scale. Black contour shows isopycnals

two points, ~ 10 km, the current velocity of the Kuroshio ~ 2 ms^{-1}, and the increase of nitrate concentration 2.2 μM, which is assumed to occur in a few meter thick vertical layer, yield the nitrate flux of $> \mathcal{O}(10$ mmol N m^{-2}day$^{-1})$. Our estimated nitrate diffusive flux of $> \mathcal{O}(1$ mmol N m^{-2}day$^{-1})$ is 10 times less than that in Hasegawa et al. (2004). This is probably because our float measurements started away from these shallowest parts in the ridge to avoid the direct bottom contact by the float, while their measurements are very close to Aoga-shima Island, and because the increase in nitrate concentration they found can also be attributed to the upwelling behind the island. On the other hand, Tanaka et al. (2016) reported the nitrate diffusive flux of $\mathcal{O}(1$ mmol N m^{-2}day$^{-1})$ in 50–150 m depth above the sill near Mikura-jima Island in the Izu Ridge (Fig. 1a), which is a similar magnitude to our estimates in this study. However, because these previous estimates of nitrate diffusive flux are limited to regions very

close to the topographic features, it was unclear how long the elevated nutrient flux persists toward the downstream direction. Considering our profiling measurements started several tens of kilometers away from the shallowest topographic features in the Izu Ridge, the results suggest that the elevated nitrate flux of $\mathcal{O}(1$ mmol N m^{-2}day$^{-1})$ in 50–125 m depth persists over about 100 km from the shallowest part of the Izu Ridge along the Kuroshio toward the downstream regions.

This elevated nutrient flux is expected to increase primary production in the downstream. From the region 200 km away from the south-westernmost part of the transect, the measured chlorophyll-a concentration by the Navis-BGC float shows larger values, 0.75–1.2 μgL^{-1} to the downstream direction than the upstream values, 0.3–0.5 μgL^{-1} (Fig. 4a). The maximum value of the chlorophyll-a concentration coincides with the low salinity water interleaving, implying the
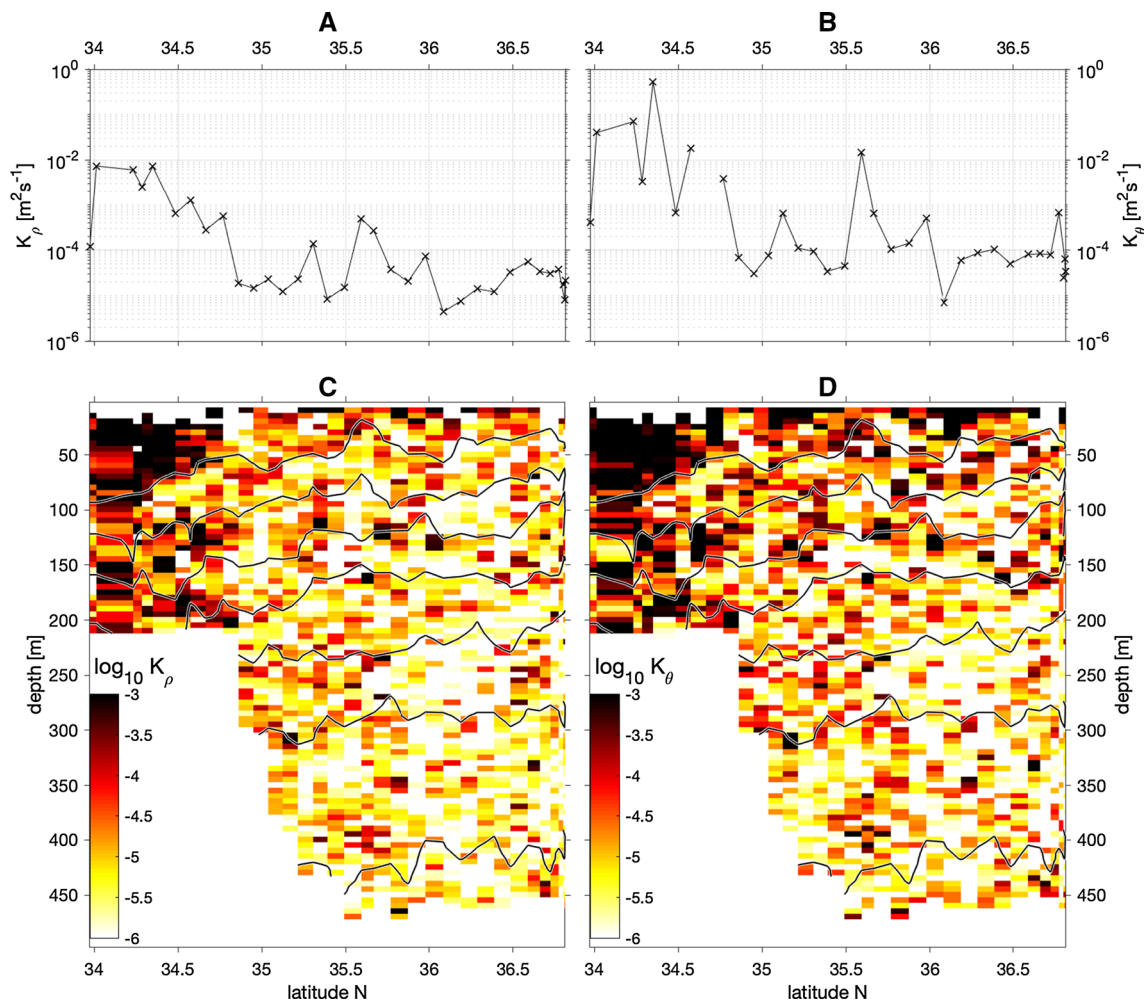
Fig. 7 Vertical eddy diffusivity, K_ρ [m²s⁻¹] and effective thermal diffusivity K_θ [m²s⁻¹]. Mean (**a**) K_ρ and (**b**) K_θ averaged between 40 and 200 m depth as a function of latitude. Vertical sections for (**c**) K_ρ and (**d**) K_θ. The values are shown in log scale. Black contour shows isopycnals

advection of cold-fresh chlorophyll-a rich water. However, temperature–salinity diagram shows that water property measured by the Navis-BGC float is close to the Kuroshio warm-salty water and that chlorophyll-a concentration is rather independent on salinity (Fig. 5) with the small negative correlation coefficient, -0.3. Thus, although there are some advective effects of cold-fresh chlorophyll-a rich water, the observed increases in the chlorophyll-a concentration in the downstream region cannot simply be explained by the advection effects. Instead, considering the current velocity of the Kuroshio, $\mathcal{O}(1\,\mathrm{ms^{-1}})$, it takes 1–2 days to travel a distance of 200 km, which is similar time scale to the phytoplankton doubling time. Therefore, increased subsurface chlorophyll-a concentration in the downstream region of the Izu Ridge, can plausibly be explained by the elevated nutrient flux in the Kuroshio near the Izu Ridge.

In this region near the Izu Ridge, two estimates of the diffusive nutrient flux based on the eddy diffusivity K_ρ and the effective thermal diffusivity K_θ are nearly identical (Fig. 9).

The similarity between K_ρ and K_θ and associated fluxes suggests that microscale mixing is dominated by turbulence. Mechanisms of the turbulent mixing is, however, not clear because our profiling float data during June 2017 cruise lack velocity measurements. One possible mechanism is internal tides. Because, the Izu Ridge is known to generate large amplitude internal tides, freely propagating semidiurnal internal tides and bottom trapped diurnal internal tides can induce strong turbulence near their generation sites (Niwa and Hibiya 2011). The Navis-MR float was deployed during the neap tide near Izu Ridge and recovered during the spring tide in the Kuroshio Extension. Therefore, the effects from the tides on the observed mixing can be considered to be relatively weak. The strong turbulence measured in the region close to the Izu Ridge is caused also by the Kuroshio flowing over shallow sills. When the strong geostrophic currents encounter the bottom topography, previous studies show that lee waves and hydraulic jump occur and cause strong turbulent mixing in the vicinity of the topographic
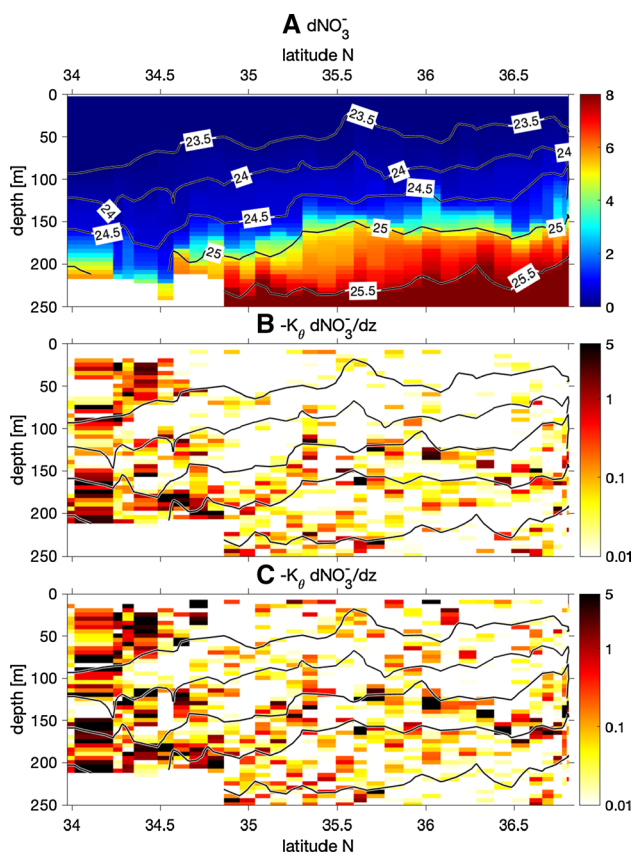
Fig. 8 Vertical sections of (**a**) nitrate concentration [μ M], diffusive flux with (**b**) eddy diffusivity $F_\rho^{NO_3^-}$ and with (**c**) effective thermal diffusivity $F_\theta^{NO_3^-}$, $\log_{10}$[mmol N m^{-2}day^{-1}]

features (e.g., Nikurashin and Ferrari 2011). In addition, the previous observational study in the Tokara Strait, where the Kuroshio flows over many seamounts showed that the large TKE dissipation rates are associated with the high vertical wave number near-inertial internal wave shear (Nagai *et al.* 2017). Near-inertial waves are known to be generated by atmospheric disturbances (D'Asaro and Perkins 1984). Several studies have shown that geostrophic flow over topography leads to inertial oscillation (Nikurashin and Ferrari 2010; Vadas and Fritts 2001; Lott 2003). Also, a few numerical studies have shown that they are generated from the meandering fronts (Nagai et al. 2015a; Shakespeare and Hogg 2017). Regardless of their generation mechanisms, the near-inertial waves are trapped in the region of negative relative vorticity and the layer of strong geostrophic vertical shear (Kunze 1985; Whitt and Thomas 2013; Mooers 1975). Because the float measurements were made in the Kuroshio with the large geostrophic lateral and the vertical shear, the observed relatively high TKE dissipation rates may be attributed to the trapped near-inertial waves in the Kuroshio Front.

Although K_ρ- and K_θ-derived diffusive fluxes are nearly identical, there are some exceptions. They differ significantly

in the region at 35.5–36°N where the low salinity interleaving layer is observed (Fig. 3 and 9). When diffusion is caused by microscale turbulence, density and heat are diffused equally with two diffusivities for density K_ρ and heat K_θ being nearly identical. On the other hand, the double-diffusive convection exchanges temperature and salinity differently while generating new density layers as oppose to the density diffusion. Therefore, unlike turbulence, two diffusivities for density K_ρ and heat K_θ should be different in the double-diffusive layers. Also because eddy diffusivity for density K_ρ obtained with the measured TKE dissipation rate ϵ is based on an assumption that 17% of the TKE shear production is consumed for destructing the density stratification, it is most likely overestimating the true K_ρ in the double-diffusive layers. On the other hand, because the double-diffusive convection produces rich microscale thermohaline structures caused by salt-fingers and diffusive convection without strong turbulence, a much larger measured thermal diffusivity than the measured eddy diffusivity can be a useful indicator to detect active double-diffusive convection (Nagai et al. 2015b).

Accordingly, it is examined if the larger effective thermal diffusivities K_θ than eddy diffusivities for density K_ρ in the regions 34–34.4°N and 35.5–36°N can be attributed to double-diffusive convection. The Turner angle Tu computed using measured temperature and salinity (7) by Navis-MR shows salt finger favorable values ($45 < Tu < 90°$) frequently near the salinity interleaving layers in 50–125 m depth (Fig. 3) with some diffusive convection favorable values ($-90 < Tu < -45°$) near the surface and in the southwesternmost part below 100 m depth (Fig. 13). It should be noted that the relatively large $Tu > 60°$ is found periphery of the low salinity interleaving structure at 35.5–36°N (Figs. 3 and 13). In these salt-finger favorable interleaving layers, the buoyancy Reynolds number Re_b is mostly less than 20, suggesting that turbulence is too weak to induce buoyancy vertical flux (Yamazaki 1990). Accordingly, the larger diffusive nutrient flux derived by the effective thermal diffusivity K_θ than that by the eddy diffusivity for density K_ρ in 50–125 m depth at 35.5–36°N (Fig. 9) could be attributed to the salt-finger above the low salinity water interleaving. In the regions 34–34.4°N, larger K_θ than K_ρ is found below 100 m depth and above 50 m depth (Fig. 7c–d). In these locations, Tu shows also double-diffusion favorable values accompanied mostly by the small buoyancy Reynolds number (Fig. 13). However, because the buoyancy Reynolds number is very large above 100 m depth, which suggests the domination of turbulence, the associated diffusive nutrient fluxes averaged in 50–125 m depth with K_ρ and K_θ show similar values (Fig. 9).

Although there are some exceptions, the turbulent diffusion is found to play a dominant role in supplying nutrients toward surface layers across the density layers in the

Fig. 9 Nutrient diffusive flux [mmol m^{-2}day^{-1}] averaged in 50–125 m depth as a function of latitude for (**a**) nitrate and (**b**) phosphate. Black indicates diffusive flux computed with the eddy diffusivity K_ρ ($F_\rho^{NO_3^-}$ and $F_\rho^{PO_4^{3-}}$) for density and red represents that with the effective thermal diffusivity K_θ ($F_\theta^{NO_3^-}$ and $F_\theta^{PO_4^{3-}}$). Shading represents 95% confidence interval
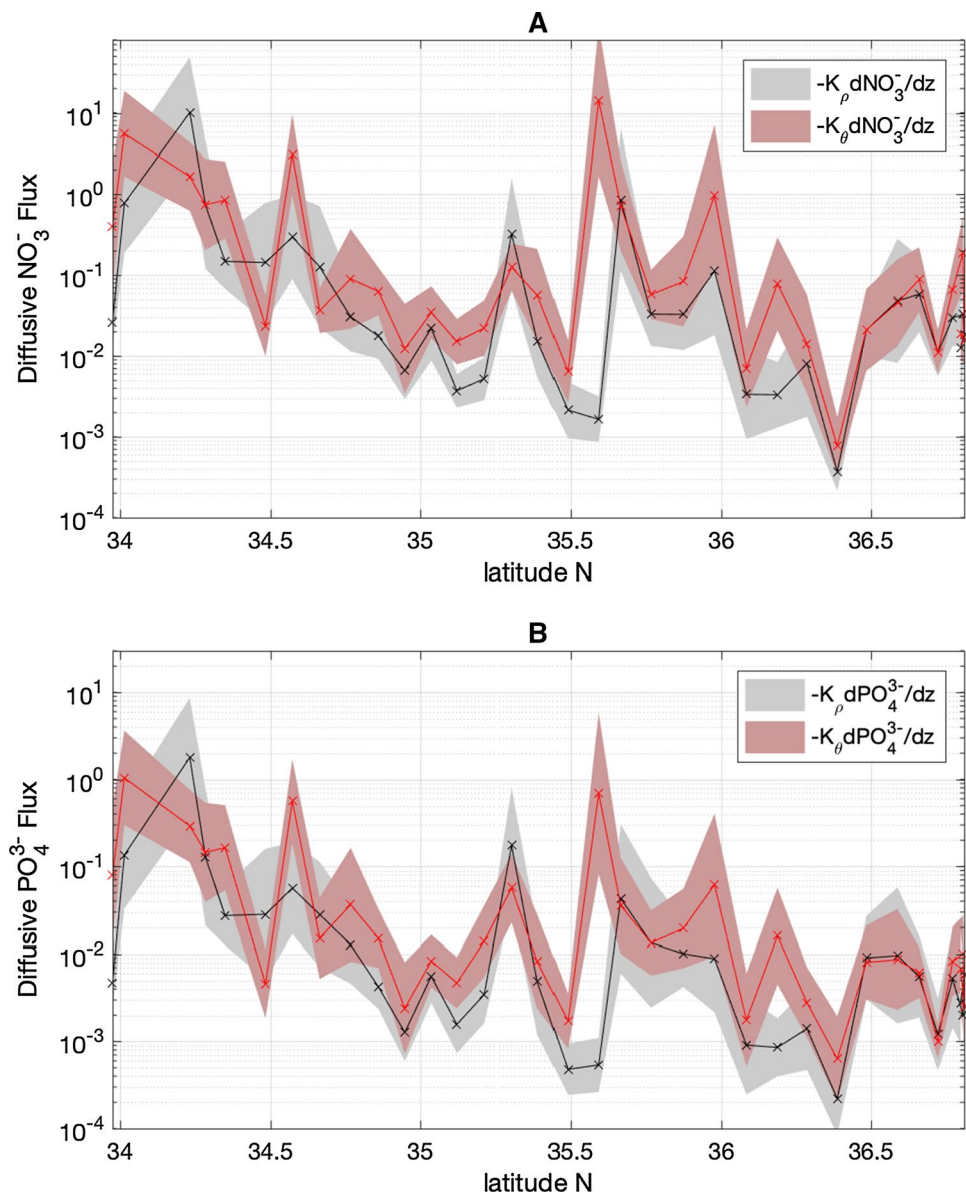
Kuroshio near the Izu Ridge. In contrast, continuous profiling observations using autonomous floats in the Kuroshio Extension revealed that the double-diffusive convection is the dominant agent to induce the diapycnal diffusive flux of nitrate in and below the thermocline. The double-diffusive favorable conditions can be generated by lateral stirring and entrainment of cold-fresh Oyashio influenced waters into the warm-salty Kuroshio waters. The water property shown in the temperature and salinity diagram illustrates that spiciness is greatly increased in the Kuroshio Extension compared to that in the Kuroshio across the Izu Ridge, although these observations are conducted in the different years (Fig. 5). The Navis-MR microstructure float data show 10–100 times larger nitrate diffusive fluxes of 1-10 mmol N m^{-2}day^{-1} with the effective thermal diffusivity K_θ than that with K_ρ in 150–300 m. In these layers, σ_θ

is 26–26.5 kgm^{-3} which is near the core of the Kuroshio nutrient stream (Guo et al. 2012). Therefore, the observed double-diffusion-induced nitrate flux can diffuse up the nitrate from the core of the nutrient stream to the shallower layers. These values of the double-diffusive nitrate flux are 1–2 orders of magnitude larger than that estimated by Oschlies et al. (2003) and Dietze et al. (2004). However, this pycnostad (σ_θ 26–26.5 kgm^{-3}) does not outcrop along the Kuroshio Extension even during winter seasons. Therefore, the nutrients diffused up by the double diffusion, which then transported to the north through the lateral stirring caused by rich mesoscale eddies and submesoscale flows in the Kuroshio Extension regions, can generate the upward eddy flux (Lee and Williams 2000) or induction flux (Williams and Follows 2006) in the region north from the Kuroshio
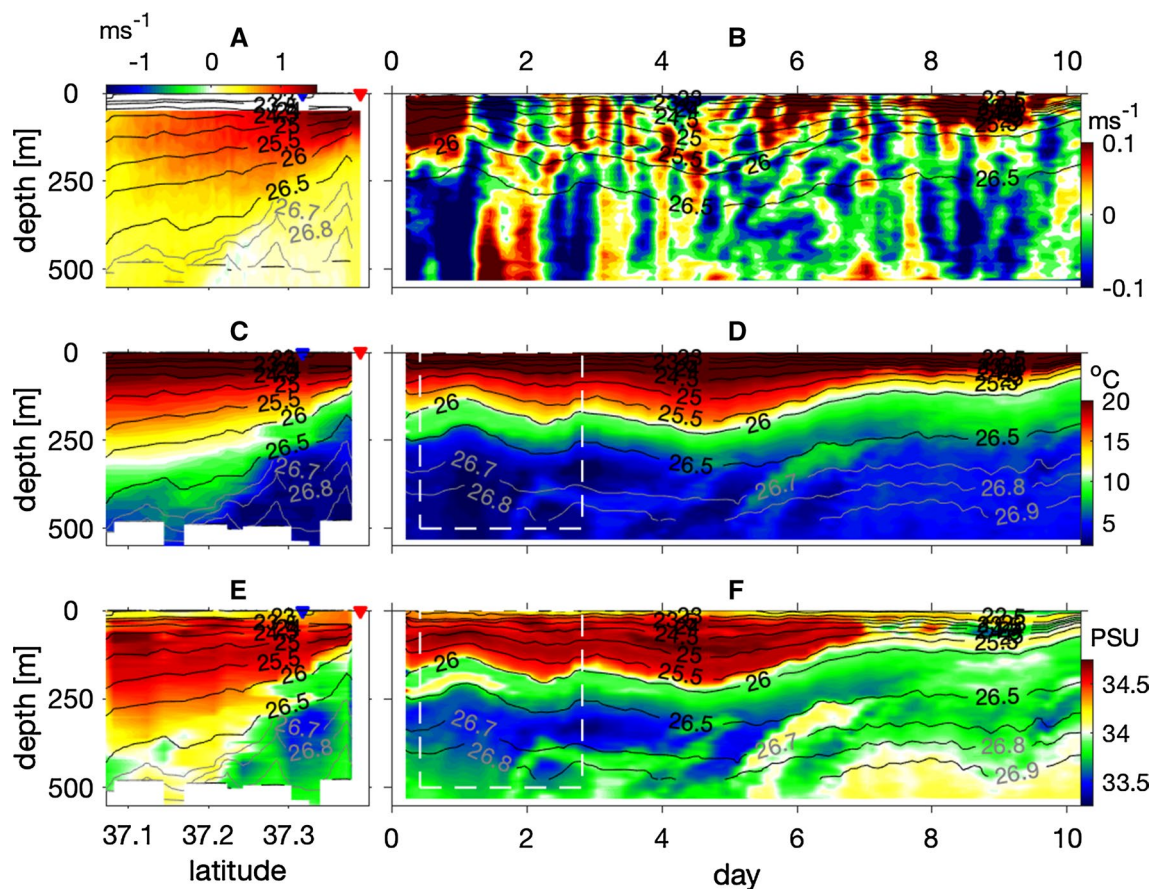
Fig. 10 Vertical sections of (**a**) along Kuroshio Front flow, (**b**) across-front flow, (**c**–**d**) temperature, and (**e**–**f**) salinity. (**a**, **c**, **e**) show across frontal sections obtained by the Underway-CTD observations. (**b**, **d**, **f**) are along frontal sections measured by EM-APEX float. Black contours are isopycnals. Dashed-white box in (**d**) and (**f**) are the region measured by the Navis-MR microstructure float. Blue and red triangles in (**a**, **c**, **e**) indicate the deployment positions for the Navis-MR and the Navis-BGC floats, respectively

Extension (Nagai et al. 2019a). The nutrients transported to the south by eddy, on the other hand, are subducted to the deeper layer and recirculated into the subsurface subtropical gyre (Pelegrí and Csanady 1991; Nagai et al. 2015c; Pelegrí et al. 2019).

Although our microstructure float data showed the importance of the double diffusion in diapycnal nutrient flux in the Kuroshio Extension, the deployment range is limited to only 300 km along the Kuroshio Extension. It is not clear how long the double-diffusion-induced nutrient flux continues toward the further downstream direction. In addition to the Navis-MR float, we deployed the EM-APEX float along nearly the same trajectory as the Navis-MR but over 900 km distance in the Kuroshio Extension. This long-distance high-frequency continuous profiling revealed wide-spread double-diffusive favorable thermohaline interleaving structures (Fig. 10c–f and 11A). Although the EM-APEX float does not carry the microstructure sensors, high-resolution temperature and salinity data allow us to estimate the double-diffusion-induced diffusivity using

the parameterizations developed by Radko and Smith (2012) for salt-finger and Fedorov (1988) for diffusive convection. The parameterized double-diffusion-induced thermal diffusivity shows enhanced values in and below the thermocline over 900 km, where the thermohaline interleaving layers are observed. The Richardson number Ri computed using horizontal flow data and the standard CTD measurements by the EM-APEX float show $Ri > 0.25$, implying that these subsurface layers are stable for Kelvin–Helmholtz instability, and that double diffusion may not be disrupted by turbulence. On the other hand, it has been shown previously that the double-diffusion-induced effective thermal diffusivity is relatively larger than that for salt with the same density ratio, R_ρ (Kelley 1984). Therefore, it remains somewhat unclear which diffusivity is better to use for estimating the nutrient flux and how accurate the estimated nutrient flux is. However, because these two diffusivities show similar orders of magnitude at $R_\rho \sim 1$ (Kelly 1984) and because our microstructure profiler could obtain the effective diffusivity for heat but not for salt, the effective

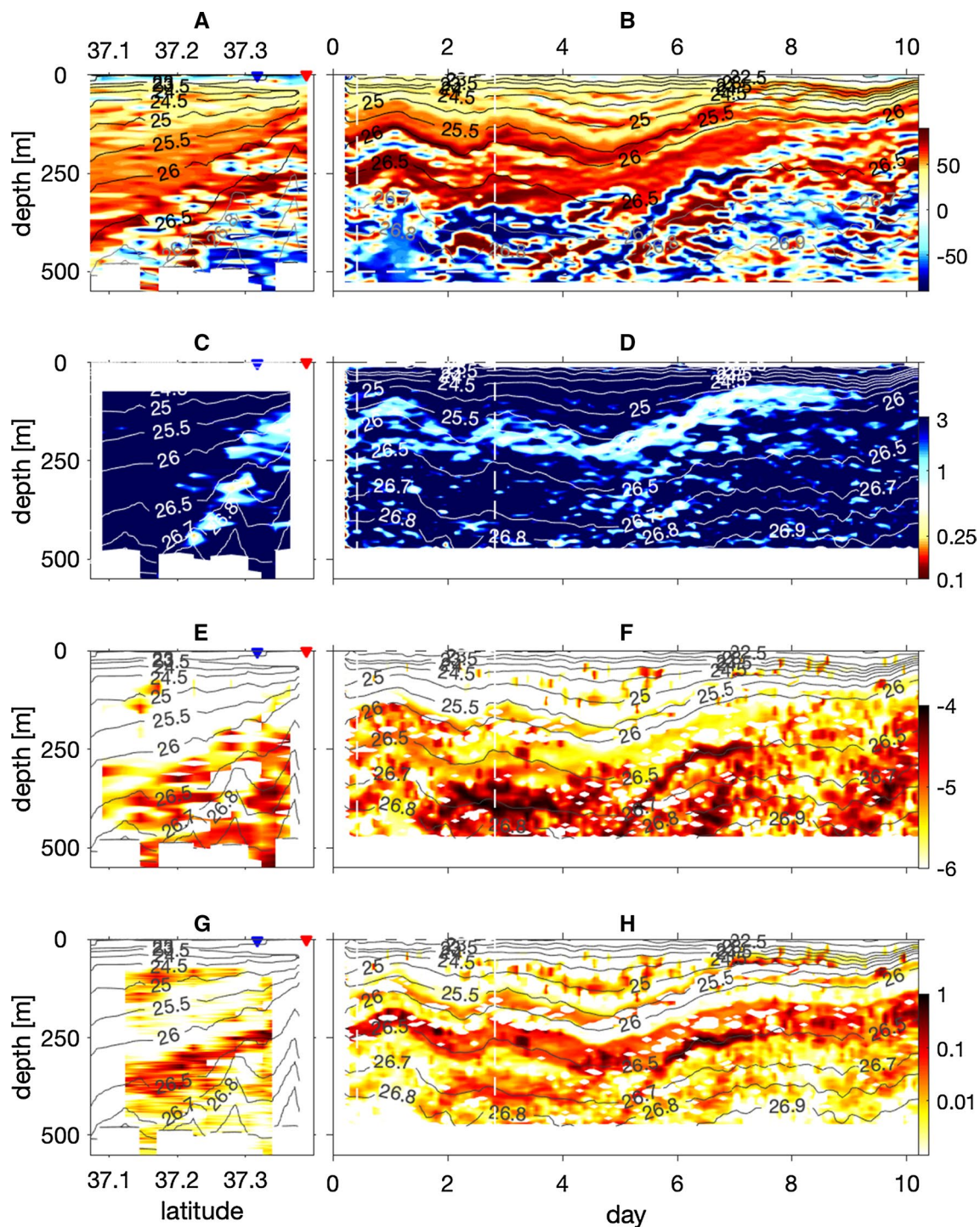**Fig. 11** Vertical sections of (**a–b**) Turner angle, *Tu* [°], (**c–d**) gradient Richardson number, (**e–f**) parameterized thermal diffusivity for double diffusion [m²s⁻¹], and (**g–h**) are parameterized double-diffusive thermal diffusivity is used to estimate the nitrate flux [mmol N m⁻²day⁻¹]. Blue and red triangles in (**a**, **c**, **e**, **g**) indicate the deployment positions for the Navis-MR and the Navis-BGC floats, respectively

thermal diffusivity is used to estimate the nitrate flux. The previous studies have also suggested that the effect of the vertical shear of the background flows, which is not considered in the parameterization used in this study, can prevent

the development of the salt-finger (Kunze 2003), suggesting that the parameterized diffusivity without considering the shear effect could overestimate the diffusivity. However, the orders of magnitude of the parameterized diffusivity are $\mathcal{O}$
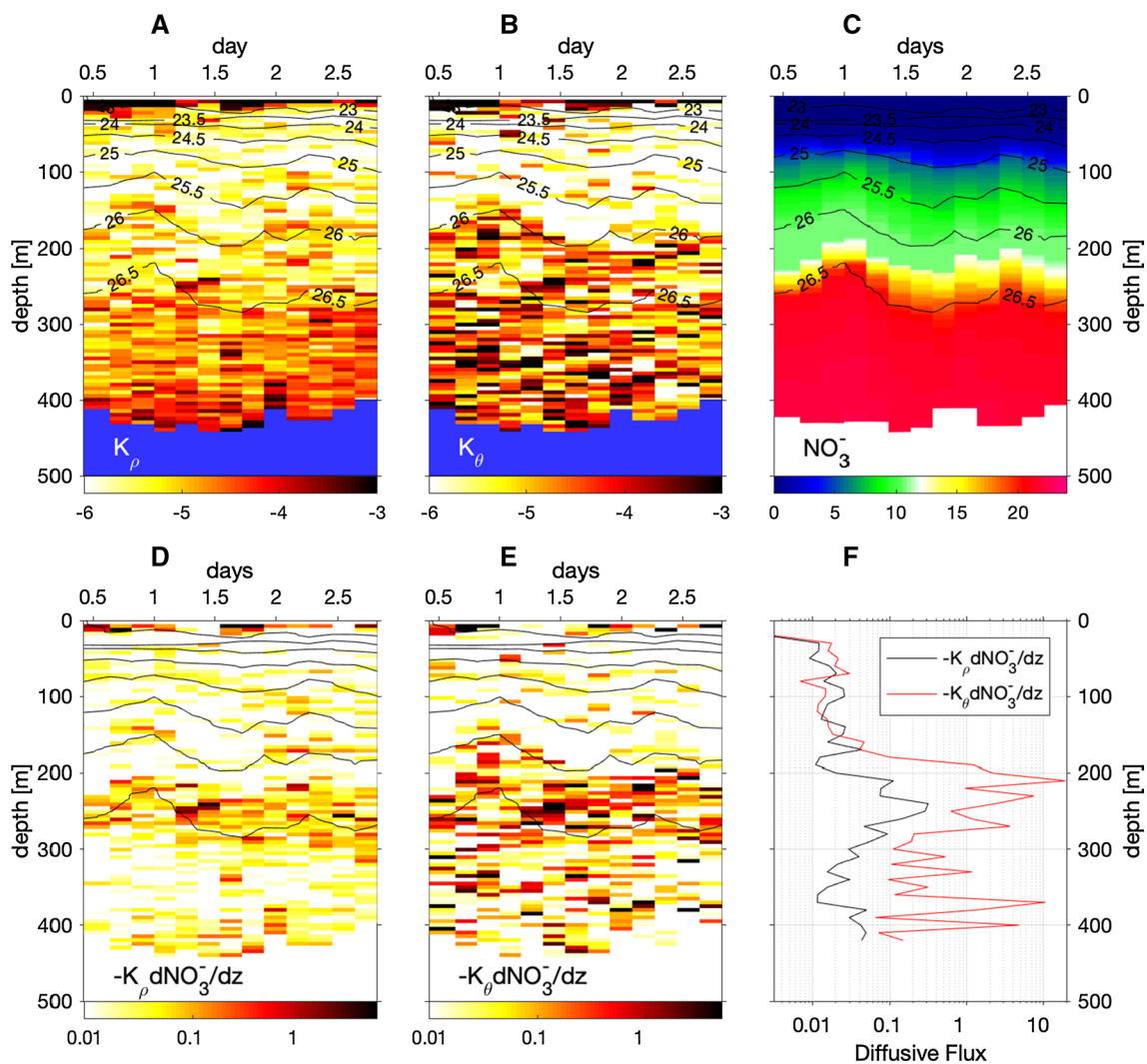
Fig. 12 Microstructure and turbulence data obtained by the Navis-MR float along the Kuroshio during July 2013 cruise. The trajectory and the measured depth range of the float are shown in Fig. 1 and Fig. 10. **a** Eddy diffusivity for density K_ρ $\log_{10}[m^2 s^{-1}]$ using TKE dissipation rates ϵ $[W kg^{-1}]$. **b** Effective thermal diffusivity K_θ $\log_{10}[m^2 s^{-1}]$. **c** Estimated nitrate concentration $[\mu M]$. **d** Nitrate diffusive flux by turbulence $F_\rho^{NO_3^-}$ and (**e**) double-diffusive nitrate flux $F_\theta^{NO_3^-}$ $[mmol\,N\,m^{-2} day^{-1}]$. **f** Average diffusive nitrate flux for (black) $F_\rho^{NO_3^-}$ and (red) $F_\theta^{NO_3^-}$ $[mmol\,N\,m^{-2} day^{-1}]$

$(10^{-5}–10^{-4}\ m^2 s^{-1})$ (Fig. 11e–f), an order smaller than the measured effective thermal diffusivity $\mathcal{O}(10^{-4}–10^{-3}\ m^2 s^{-1})$ (Fig. 12b). The parameterized double-diffusion-induced nitrate flux also shows elevated values in and below the thermocline over 900 km but with $0.1–1\ mmol\,N\,m^{-2} day^{-1}$ (Fig. 11g–h), which are also an order magnitude smaller than those estimated using the measured effective thermal diffusivity K_θ, i.e., $F_\theta^{NO_3^-} \sim 1–10\ mmol\,N\,m^{-2} day^{-1}$ (Fig. 12e–f). The relatively smaller parameterized thermal diffusivity than the observed one, seen in the region of the Navis-MR measurements implies that the parameterized double-diffusion-induced diffusive nitrate flux underestimates the actual flux

by an order of magnitude. Because the elevated values in the parameterized nitrate flux at 150–300 m depth spreads entire section over 900 km, the large diffusive nitrate flux of $1–10\ mmol\,N\,m^{-2} day^{-1}$ found by the Navis-MR data can be persistent features of the Kuroshio Extension over a 1000 km along frontal distance.

Although these very large thermal diffusivity values accompanied by the double-diffusive favorable thermohaline distributions are observed, once double-diffusive convection reaches its equilibrium, the diffusive flux of nutrients should decrease quickly. However, these thermohaline interleaving structures are found to be
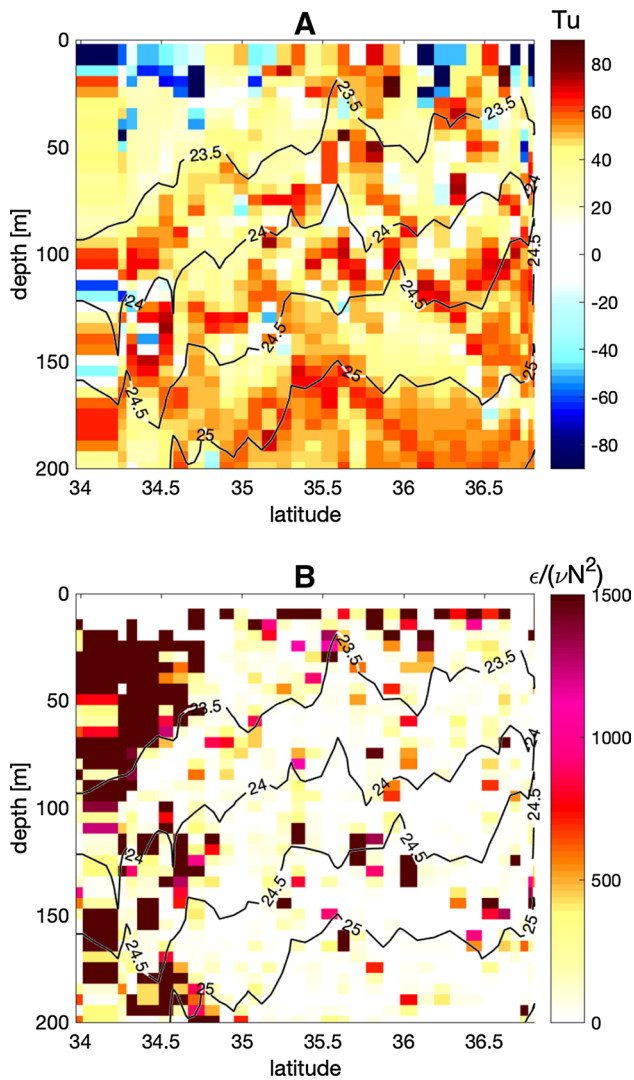
Fig. 13 Vertical section of (**a**) Tuner angle, *Tu* (7) and (**b**) buoyancy Reynolds number, Re_b (11)

generated by vertical shear of the continuous meso- and submesoscale stirrings and by near-inertial internal wave shear. Therefore, these subinertial and near-inertial flows and shear can continuously renew the double-diffusive favorable thermohaline distributions over a timescale much longer (days to weeks) than that for the double-diffusive convection (minutes to hours). In other words, this vertical shearing of the thermohaline interleaving layers continuously forms the double-diffusion favorable interleaving that are kept being diffused vertically by the enhanced double-diffusive convection. This is consistent with the results from a high-resolution numerical simulation by Nagai and Clayton (2017), in which they found nitrate interleaving layers caused by subinertial ageostrophic shear and near-inertial wave shear, though the latter near-inertial shear merely stretches and squeezes

laterally the nitrate back and forth without producing the net flux of nitrate. However, the model of Nagai and Clayton (2017) did not consider double diffusion at all. If there is a diapycnal mixing process to diffuse these tracer interleaving layers, the periodic shearing by near-inertial waves should be able to produce a net transport through the shear dispersion (Young and Garrett 1982; Kunze and Sundermeyer 2015). Our results based on the direct microstructure observations suggest that the double diffusion is responsible for diffusing the tracer interleaving vertically in the interior layers of the Kuroshio Extension.

5 Summary and conclusions

In this study, the data from two observational campaigns conducted during July 2013 and June 2017 are analyzed. In both the surveys, an autonomous microstructure profiling float, a Navis-MR was deployed in the Kuroshio flowing over the Izu Ridge and the Kuroshio Extension with other autonomous floats such as a Navis-BGC float, which carries biogeochemical sensors, and an EM-APEX float which can measure horizontal current velocity.

The float measurements in the Kuroshio near the Izu Ridge show elevated turbulent kinetic energy dissipation rates of $> \mathcal{O}(10^{-7}\,\mathrm{W\,kg^{-1}})$ in upper 200 m depth in the region close to the Izu Ridge (Fig. 6a). The strong turbulence induces elevated nitrate diffusive flux of 1-10 mmol N m^{-2}day^{-1} (Figs. 8 and 9a). These elevated TKE dissipation rates and diffusive nitrate flux are persistently found in the region 100 km from the Izu Ridge toward the downstream direction. The large nutrient diffusive flux near the Izu Ridge seems to induce subsurface phytoplankton growth inside the Kuroshio in the downstream region 200 km from the Izu Ridge.

After the Kuroshio Current is separated from the coast, it continues as the eastward flowing Kuroshio Extension. Along the Kuroshio Extension, the measured temperature and salinity data show more influences from the cold-fresh Oyashio related waters than that along the northeastward flowing Kuroshio south of Japan. The vertical shearing of cold-fresh Oyashio related water, caused by the meso- and submesoscale lateral stirring and near-inertial waves, can lead to the generations of the double-diffusion favorable thermohaline interleaving layers in and below the thermocline of the Kuroshio Extension over 900 km. The measured TKE dissipation rates, using the Navis-MR float, show that turbulence is not strong enough to disrupt the double-diffusive convection in these thermohaline interleaving layers. On the other hand, the measured microscale thermal variance dissipation rates show very large values, resulting in the 1–2 orders of magnitude larger measured effective thermal

diffusivity K_θ than the eddy diffusivity for density K_ρ in these thermohaline interleaving layers. The nitrate diffusive fluxes, estimated with the effective thermal diffusivity K_θ and the eddy diffusivity for density K_ρ, also show 1–2 orders of magnitude larger values with K_θ than that with K_ρ.

These results suggest that the dominant agent for the diapycnal nutrient flux is turbulent mixing caused by a flow over the topography in the Kuroshio near the Izu Ridge, whereas it is double-diffusive convection in the Kuroshio Extension region. The former diffusive nutrient flux seems to reach surface layers depending on how shallow the topography that the Kuroshio interferes is, while the latter seems to be in the subsurface layers of $\sigma_\theta = 26$–$26.5\,\mathrm{kgm}^{-3}$ based on the results of the observations of this study. If the latter double-diffusive flux is limited in these subsurface density layers, whether the diffused nutrients by double diffusion become available depends on how they are stirred laterally by meso- and submesoscale flows with the northward eddy flux resulting in the upward nutrient supply and the southward eddy flux leading to the subduction and recirculation to subsurface layers of the subtropical gyre (Lee and Williams 2000; Pelegrí and Csanady 1991). How much fraction is ultimately supplied to the northern surface and subducted to the southern depth should be subjects of the future studies.

The reported effects of the mixing induced by the currents over the topography, and fine-scale thermohaline interleaving and associated microscale double diffusion are currently missing in the climate and many regional models due to the coarse lateral and vertical resolutions. Because the nutrient diffusive flux caused by these multiscale processes are found to be 1–2 orders of magnitude larger than that previously estimated, and because it persists a long distance of 100–1000 km along the current, they should be taken into account in those models to accurately predict the ecosystem responses to the expected climate changes.

References

Chang M-H, Jheng S-Y, Lien R-C (2016) Trains of large Kelvin-Helmholtz billows observed in the Kuroshio above a seamount. Geophys Res Lett 43(16):8654–8661. https://doi.org/10.1002/2016GL069462

D'Asaro E, Perkins H (1984) A near-inertial wave spectrum for the Sargasso Sea in late summer. J Phy Oceanogr 14:489–505

Dietze H, Oschlies A, Kähler P (2004) Internal-wave-induced and double-diffusive nutrient fluxes to the nutrient-consuming surface layer in the oligotrophic subtropical North Atlantic. Ocean Dynam 54(1):1–7. https://doi.org/10.1007/s10236-003-0060-9

Durán Gómez GS , Nagai T, Yokawa K (2020) Mesoscale warm-core eddies drive interannual modulations of swordfish catch in the Kuroshio Extension System. Front Marine Sci https://doi.org/10.3389/fmars.2020.00680

Fedorov KN (1988) Layer tickles and effective diffusivities in diffusive thermohaline convection in the ocean. In: Nihoul J, Jamart B (eds) Small-scale turbulence and mixing in the ocean. Elsevier, Amsterdam

Flament P (2002) A state variable for characterizing water masses and their diffusive stability: spiciness. Progress in Oceanography 54(1), 493 - 501. http://www.sciencedirect.com/science/article/pii/S0079661102000654 (Observations of the 1997-98 El Nino along the West Coast of North America) https://doi.org/10.1016/S0079-6611(02)00065-4

Guo X, Zhu XH, Wu QS, Huang D (2012) The Kuroshio nutrient stream and its temporal variation in the East China Sea. Global Biogeochem Cycles 117:C01026. https://doi.org/10.1029/2011JC007292

Guo X, Zhu XH, Long Y, Huang D (2013) Spatial variations in the Kuroshio nutrient transport from the East China Sea to south of japan. Biogeosciences 10:6403–6417

Hasegawa D (2019) Island mass effect. In: Kuroshio Current (p. 163-174). American Geophysical Union (AGU). https://doi.org/10.1002/9781119428428.ch10

Hasegawa D, Yamazaki H, Lueck RG, Seuront L (2004) How islands stir and fertilize the upper ocean. Geophys Res Lett. https://doi.org/10.1029/2004GL020143

Hashihama F (2013) A biogeochemical study in surface waters of the subtropical ocean using a highly-sensitive method for measuring nanomolar nutrients. Oceanography Japan 22:169–185. https://doi.org/10.5928/kaiyou.22.5_169

Hashihama F, Furuya K, Kitajima S, Takeda S, Takemura T, Kanda J (2009) Macro-scale exhaustion of surface phosphate by dinitrogen fixation in the western north pacific. Geophys Res Lett. https://doi.org/10.1029/2008GL036866

Kaneko H, Yasuda I, Komatsu K, Itoh S (2012) Observations of the structure of turbulent mixing across the Kuroshio. Geophys Res Lett. https://doi.org/10.1029/2012GL052419

Kaneko H, Yasuda I, Komatsu K, Itoh S (2013) Observations of vertical turbulent nitrate flux across the Kuroshio. Geophys Res Lett 40:3123–3127. https://doi.org/10.1002/grl.50613

Kelley D (1984) Effective diffusivities within oceanic thermohaline staircases. J Geophys Res 89:10484–10488

Kobari T, Honma T, Hasegawa D, Yoshie N, Tsutsumi E, Matsuno T, ... Nakamura H (2020) Phytoplankton growth and consumption by microzooplankton stimulated by turbulent nitrate flux suggest rapid trophic transfer in the oligotrophic Kuroshio. Biogeosciences 17(9), 2441–2452. https://bg.copernicus.org/articles/17/2441/2020/https://doi.org/10.5194/bg-17-2441-2020

Komatsu K, Hiroe Y (2019) Structure and impact of the Kuroshio nutrient stream. In: Nagai Takeyoshi, Saito Hiroaki, Suzuki Koji, Takahashi Motomitsu (eds) Kuroshio Current: Physical,

Biogeochemical and Ecosystem Dynamics, AGU Geophysical Monograph Series. AGU-Wiley, New York

Kraichnan R (1968) Small-scale structure of a scalar field convected by turbulence. Phys Fluids 11:945–953

Kunze E (1985) Near-inertial wave propagation in geostrophic shear. J Phys Oceanogr 15:544–565

Kunze E (2003) A review of oceanic salt fingering theory. Prog Oceanogr 56:399–417

Kunze E, Sundermeyer MA (2015) The Role of Intermittency in Internal-Wave Shear Dispersion. J Phys Oceanogr 45(12):2979–2990. https://doi.org/10.1007/s10236-003-0060-90

Lee M-M, Williams RG (2000) The role of eddies in the isopycnic transfer of nutrients and their impact on biological production. J Mar Res 58:895–917

Lott F (2003) Large-scale flow response to short gravity waves breaking in a rotating shear. J Atmos Sci 60:1691–1704

Mooers CN (1975) Several effects of baroclinic current on the cross-stream propagation of inertial-internal waves. Geophys Fluid Dyn 6:245–275

Nagai T, Clayton S (2017) Nutrient interleaving below the mixed layer of the Kuroshio Extension Front. Ocean Dynamycs 67:1027–1046

Nagai T, Tandon A, Yamazaki H, Doubell MJ (2009) Evidence of enhanced turbulent dissipation in the frontogenetic Kuroshio Front thermocline. Geophys Res Lett 36:L12609. https://doi.org/10.1007/s10236-003-0060-96

Nagai T, Tandon A, Yamazaki H, Doubell MJ, Gallager S (2012) Direct observations of microscale turbulence and thermohaline structure in the Kuroshio Front. J Geophys Res 117:C08013. https://doi.org/10.1007/s10236-003-0060-97

Nagai T, Tandon A, Kunze E, Mahadevan A (2015a) Spontaneous generation of near-inertial waves by the Kuroshio Front. J Phys Oceanogr 45:2381–2406. https://doi.org/10.1007/s10236-003-0060-95

Nagai T, Inoue R, Tandon A, Yamazaki H (2015b) Evidence of enhanced double-diffusive convection below the main stream of the Kuroshio Extension. J Geophys Res 120:8402–8421. https://doi.org/10.1007/s10236-003-0060-94

Nagai T, Gruber N, Frenzel H, Lachkar Z, McWilliams JC, Plattner G-K (2015c) Dominant role of eddies and filaments in the offshore transport of carbon and nutrients in the California Current System. J Geophys Res. https://doi.org/10.1007/s10236-003-0060-92

Nagai T, Hasegawa D, Tanaka T, Nakamura H, Tsutsumi E, Inoue R, Yamashiro T (2017) First evidence of coherent bands of strong turbulent layers associated with high-wavenumber internal-wave shear in the upstream Kuroshio. Scient Rep. https://doi.org/10.1007/s10236-003-0060-93

Nagai T, Clayton S, Uchiyama Y (2019a) Multiscale routes to supply nutrients through the Kuroshio nutrient stream. In: Nagai Takeyoshi, Saito Hiroaki, Suzuki Koji, Takahashi Motomitsu (eds) Kuroshio Current: Physical, Biogeochemical and Ecosystem Dynamics, AGU Geophysical Monograph Series. AGU-Wiley, New York

Nagai T, Durán Gómez GS, Otero DA, Mori Y, Yoshie N, Ohgi K, Kobari T (2019b) How the Kuroshio Current delivers nutrients to sunlit layers on the continental shelves with aid of near-inertial waves and turbulence. Geophys Res Lett 46(12):6726–6735. https://doi.org/10.1007/s10236-003-0060-91

Nasmyth PW (1970) Oceanic turbulence (Unpublished doctoral dissertation). University of British Columbia, Columbia

Nikurashin M, Ferrari R (2010) Radiation and dissipation of internal waves generated by geostrophic motions impinging on small-scale topography: Theory. J Phys Oceanogr 40:1055–1074

Nikurashin M, Ferrari R (2011) Global energy conversion rate from geostrophic flows into internal lee waves in the deep ocean. Geophys Res Lett 38:L08610

Niwa Y, Hibiya T (2011) Estimation of baroclinic tide energy available for deep ocean mixing based on three-dimensional global numerical simulations. J Oceanogr 67:493–502. https://doi.org/10.1007/s10236-003-0060-98

Osborn T (1980) Estimates of the local rate of vertical diffusion from dissipation measurements. J Phys Oceanogr 10:83–89

Osborn TR, Cox CS (1972) Oceanic fine structure. Geophys Fluid Dyn 3:321–345

Oschlies A, Dietze H, Kähler P (2003) Salt-finger driven enhancement of upper ocean nutrient supply. Geophys Res Lett 30:23. https://doi.org/10.1007/s10236-003-0060-99

Pelegrí JL, Csanady GT (1991) Nutrient transport and mixing in the Gulf Stream. J Geophys Res 96:2577–2583

Pelegrí JL, Csanady GT, Martins A (1996) The North Atlantic nutrient stream. J Oceanogr 52:275–299

Pelegrí JL, Vallés-Casanova I, Orúe-Echevarría D (2019) The gulf nutrient stream. Kuroshio Current (p. 23-50). American Geophysical Union (AGU). https://doi.org/10.1002/9781119428428.ch3

Radko T (2013) Double-diffusive convection. Cambridge University Press, Cambridge

Radko T, Smith DP (2012) Equilibrium transport in double-diffusive convection. J Fluid Mech 692:5–27

Ruddick BR (1983) A practical indicator of the stability of the water column to double-diffusive activity. Deep Sea Res 30:1105–1107

Ruddick BR, Anis A, Thompson K (2000) Maximum likelihood spectral fitting: The Batchelor spectrum. J Atmos Oceanic Technol 17:1541–1555

Shakespeare CJ, Hogg AM (2017) Spontaneous surface generation and interior amplification of internal waves in a regional-scale ocean model. J Phys Oceanogr 47(4):811–826. http://www.sciencedirect.com/science/article/pii/S0079661102000654Q

Tanaka T, Hasegawa D, Yasuda I, Tsuji H, Nishioka J (2016) Enhanced vertical turbulent nitrate flux in the Kuroshio across the Izu Ridge. J Oceanogr 75:195–203. http://www.sciencedirect.com/science/article/pii/S0079661102000654l

Tsutsumi E, Matsuno T, Lien R, Nakamura H, Senjyu T, Guo X (2017) Turbulent mixing within the Kuroshio in the Tokara Strait. J Geophys Res Ocean. http://www.sciencedirect.com/science/article/pii/S0079661102000654Z

Vadas SL, Fritts D (2001) Gravity wave radiation and mean response to local body forces in the atmosphere. J Atmos Sci 58:2249–2680

Whitt D, Thomas L (2013) Near-inertial waves in strongly baroclinic currents. J Phys Oceanogr 43:706–725

Williams RG, Roussenov V, Follows M (2006) Induction of nutrients into the mixed layer and maintenance of high latitude productivity. Global Biogeochem Cycles. http://www.sciencedirect.com/science/article/pii/S0079661102000654B

Yamazaki H (1990) Stratified turbulence near a critical dissipation rate. J Phys Oceanogr 20:1583–1598

Young PBR, Garrett CJR (1982) Shearflow dispersion, internal waves and horizontal mixing in the ocean. J Phys Oceanogr 12:515–527